Supporting Information for

Understanding the Mechanical Properties of DNA Origami Tiles and Controlling the Kinetics of their Folding and Unfolding Reconfiguration

Haorong Chen[1], Te-Wei Weng[1], Molly M. Riccitelli[1], Yi Cui[2], Joseph Irudayaraj[1,2], and Jong Hyun Choi[1]*

[1]School of Mechanical Engineering, Birck Nanotechnology Center, Bindley Bioscience Center, Purdue University, West Lafayette, Indiana 47907, United States

[2]Department of Agricultural and Biological Engineering, Bindley Bioscience Center, Purdue University, West Lafayette, Indiana 47907, United States

*Email: jchoi@purdue.edu

Content

S1. Derivation of Chemical Reaction Rate Model

The reconfiguration reactions of rectangular DNA origami tiles are initiated by the addition of a set of linker strands that connect two opposite edges. There are two competing reaction pathways: oligomerization and cyclization. Their respective reaction rates depend on external parameters (i.e. temperature and concentration) as well as intrinsic properties such as structural flexibility and tile geometry. In the oligomerization reaction, multiple origami monomer tiles are linked head-to-tail into elongated oligomer ribbons, whereas the cyclization reaction produces folded cylindrical tubes through connecting the head and tail of the same origami.

The linkers were added at least 45 times more than tile monomers, therefore their concentrations were kept nearly constant throughout the experiments. The oligomerization and cyclization reaction rates are likely to be functions of linker concentration. However, since linker concentration is kept constant and abundant, this dependence produces no effect. Thus, we group the linker concentration into the association rate constant as a fixed parameter. Oligomerization can then be treated as a second-order

bimolecular reaction and cyclization as a first-order unimolecular reaction. One may think of the linkers as catalysts for these end-association reactions. For oligomerization, the forward and reverse reaction rate constants are denoted by k_a and k_d, in the unit of $nM^{-1}s^{-1}$ and s^{-1}, respectively. As a common assumption, k_a is assumed to be independent of the size of the reacting species, and every linkage has equal probability to spontaneously dissociate with a rate constant, k_d. Because cyclized species experience greater mechanical strain than flat species, the linkages in them may be easier to break, even though the linking mechanism is the same. To account for such effects, separate dissociation rate constants $k_{d,c}$ and $k_{d,f}$ are defined for cyclized and flat oligomers, respectively.

The cyclization reaction has two necessary steps: (1) the molecule (origami tiles in this case) bends into circular conformation and brings two ends into close proximity and (2) the two reactive ends join with each other. For the first-order cyclization reaction, a first-order reaction rate constant, $k_{cyclization}$, may be defined. However, this definition can obscure the two-step nature of the reaction. To better preserve the physical meaning, j-factor can be borrowed from polymerization theory[1] and DNA cyclization studies[2-5]. The j-factor (J) is defined as "the ratio of the equilibrium constants for cyclization and for bimolecular association via the cohesive ends"[5]. Therefore,

$$J = k_{cyclization} / k_a. \qquad (*)$$

J is in the unit of nM and can be understood as the effective local concentration of reactive ends. Flexible molecules or molecules that have near-circular conformation can easily bring their heads and tails to close proximity for reaction. As a result, they have larger j-factor. Generally, j-factor directly indicates the readiness of a molecule to bend into circular conformation, and can reflect the molecule's conformational information such as its flexibility and equilibrium bending angle. Oligomers of different length usually have different j-factor even though they are constructed from identical monomers. In this study, we use J to denote the j-factor of monomer tiles and J_2 for the j-factor of dimer tiles.

Species notation

F1, *F2*,..., and *Fn*: Flat oligomerized chains consisting 1,2,…,n tiles. Specially, F1 denotes flat monomer.

C1, *C2*,..., and *Cn*: Cyclized oligomer chains consisting 1, 2,…,n tiles. Specially, C1 denotes cyclized monomer.

L: A set of linker strands that connect the top and bottom edges of the origami tile.

General reaction equations

General polymerization and dissociation reactions are expressed as:

$$\mathrm{Fn} + \mathrm{Fm} + \mathrm{L} \underset{\gamma \cdot k_{d,f}}{\overset{k_a}{\rightleftharpoons}} \mathrm{F(n+m)} .$$

If $m = n$, $F(n+m)$ needs to break in the middle to yield two identical *Fn*. Thus, there is only one such linkage and γ=1. In contrast, If $m \neq n$, there are two possible linkage breaking sites for reversing the reaction, therefore γ=2.

Folding and unfolding reactions can be written as:

$$\mathrm{Fn} + \mathrm{L} \underset{n \cdot k_{d,c}}{\overset{J_n \cdot k_a}{\rightleftharpoons}} \mathrm{Cn}$$

Here, the breaking of any of the n linkages in *Cn* will cause it to unfold back into flat species. $J \cdot k_a$ is the cyclization reaction rate constant, as can be derived from equation (*). The individual j-factor value for an n-tile origami assembly is denoted by J_n. In this study, only *F1* and *F2* are observed to cyclize. Therefore, only J and J_2 are defined. Because the cyclization of *F2* is a relatively minor effect, the change of J_2 value practically does not affect the extraction of other kinetic parameters (k_a, $k_{d,c}$, and J), as shown in Figure S9.

Specific reaction equations

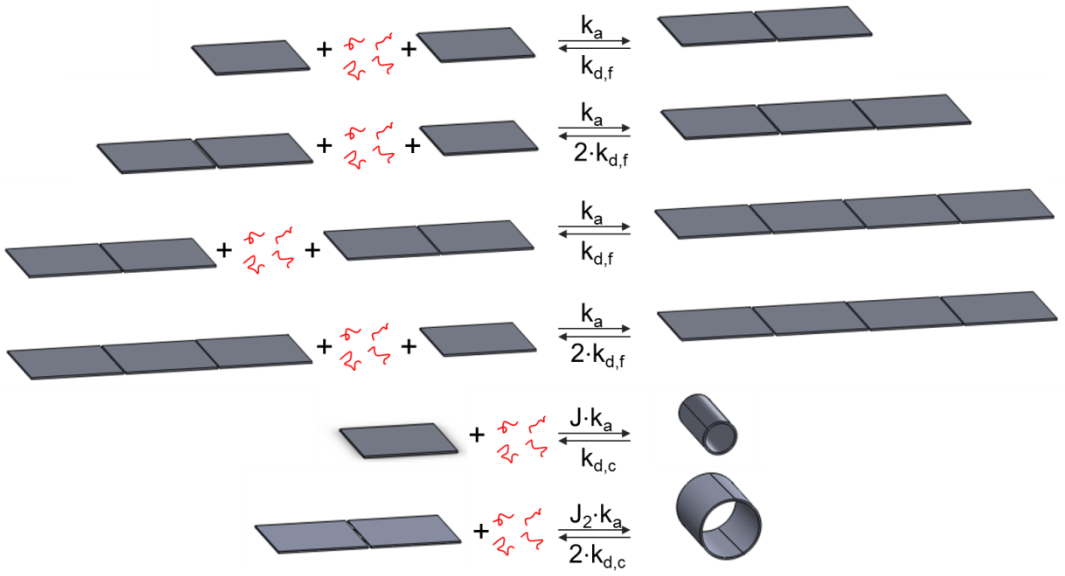

Figure S1: Schematic of the parallel reactions observed experimentally in this study. Origami tiles are in gray, Linkers are in red. *J*, k_a, k_d are a set of kinetic parameters that govern the reaction rates.

Since *F1*, *F2*, *F3*, *F4*, *C1*, and *C2* are the only species observed in AFM images, higher order species and reactions will not be considered further. As illustrated in Figure S1, there are 6 parallel reaction pathways:

$$2\ \mathrm{F1} + \mathrm{L} \underset{k_{d,f}}{\overset{k_a}{\rightleftharpoons}} \mathrm{F2} \qquad (1)$$

$$\mathrm{F2} + \mathrm{F1} + \mathrm{L} \underset{2k_{d,f}}{\overset{k_a}{\rightleftharpoons}} \mathrm{F3} \qquad (2)$$

$$2\ \mathrm{F2} + \mathrm{L} \underset{k_{d,f}}{\overset{k_a}{\rightleftharpoons}} \mathrm{F4} \qquad (3)$$

$$\mathrm{F3} + \mathrm{F1} + \mathrm{L} \underset{2k_{d,f}}{\overset{k_a}{\rightleftharpoons}} \mathrm{F4} \qquad (4)$$

$$\mathrm{F1} + \mathrm{L} \underset{k_{d,c}}{\overset{J\cdot k_a}{\rightleftharpoons}} \mathrm{C1} \qquad (5)$$

$$\mathrm{F2} + \mathrm{L} \underset{2k_{d,c}}{\overset{J_2\cdot k_a}{\rightleftharpoons}} \mathrm{C2} \qquad (6)$$

Rate equations

[*X*] denotes the concentration of species *X*. [*L*] denotes the concentration of each linker strand in the solution. The association rate constant, k_a, should be a function of [*L*]. Since [*L*] is held constant in all situation, the functional dependence have no observable effect. For simplicity, $k_a([L])$ is presented as k_a in most of the analysis.

A set of differential equations can be developed for each of the 6 reaction pathways described above.

(1) Two units of *F1* tiles associate and form *F2*.

$$\frac{d}{dt}[\mathrm{F1}]_1 = -2\cdot k_a\cdot[\mathrm{F1}]^2 + 2\cdot k_{d,f}\cdot[\mathrm{F2}]$$

$$\frac{d}{dt}[F2]_1 = k_a \cdot [F1]^2 - k_{d,f} \cdot [F2]$$

(2) One unit of *F1* and one unit of *F2* react to form one unit of *F3*. For reverse reaction, the dissociation can take place at two sites on each *F3*. Thus,

$$\frac{d}{dt}[F1]_2 = -k_a \cdot [F2] \cdot [F1] + 2k_{d,f} \cdot [F3]$$

$$\frac{d}{dt}[F2]_2 = -k_a \cdot [F2] \cdot [F1] + 2k_{d,f} \cdot [F3]$$

$$\frac{d}{dt}[F3]_2 = k_a \cdot [F2] \cdot [F1] - 2k_{d,f} \cdot [F3]$$

(3) Two identical units of *F2* react and form one unit of *F4*. The reverse reaction is the dissociation of the linkage in the middle. There is only one such site for each 4-tile chain.

$$\frac{d}{dt}[F2]_3 = -2 \cdot k_a \cdot [F2]^2 + 2 \cdot k_{d,f} \cdot [F4]$$

$$\frac{d}{dt}[F4]_3 = k_a \cdot [F2]^2 - k_{d,f} \cdot [F4]$$

(4) One unit of *F3* and one unit of *F1* react and form one unit of *F4*. For reverse reaction, there are two such linkages for each 4-tile chain.

$$\frac{d}{dt}[F1]_4 = -k_a \cdot [F3] \cdot [F1] + 2k_{d,f} \cdot [F4]$$

$$\frac{d}{dt}[F3]_4 = -k_a \cdot [F3] \cdot [F1] + 2k_{d,f} \cdot [F4]$$

$$\frac{d}{dt}[F4]_4 = k_a \cdot [F3] \cdot [F1] - 2k_{d,f} \cdot [F4]$$

(5) Cyclization reaction between two ends of the same *F1* will form *C1*. Dissociation of the linkage will turn *C1* back into *F1*.

$$\frac{d}{dt}[F1]_5 = -k_a \cdot J \cdot [F1] + k_{d,c} \cdot [C1]$$

$$\frac{d}{dt}[C1]_5 = k_a \cdot J \cdot [F1] - k_{d,c} \cdot [C1]$$

(6) Cyclization reaction between two ends of the same *F2* will form a cyclized dimer *C2*. Dissociation of either linkage in *C2* brings it back into *F2*.

$$\frac{d}{dt}[F2]_6 = -k_a \cdot J_2 \cdot [F2] + 2k_{d,c} \cdot [C2]$$

$$\frac{d}{dt}[C2]_6 = k_a \cdot J_2 \cdot [F2] - 2k_{d,c} \cdot [C2]$$

Ordinary differential equations (ODEs)

The concentration change of each species is the sum of all individual reactions. Therefore:

$$\frac{d}{dt}[F1] = \frac{d}{dt}[F1]_1 + \frac{d}{dt}[F1]_2 + \ldots + \frac{d}{dt}[F1]_6$$

$$\frac{d}{dt}[F2] = \frac{d}{dt}[F2]_1 + \frac{d}{dt}[F2]_2 + \ldots + \frac{d}{dt}[F2]_6$$

$$\frac{d}{dt}[F3] = \frac{d}{dt}[F3]_1 + \frac{d}{dt}[F3]_2 + \ldots + \frac{d}{dt}[F3]_6$$

$$\frac{d}{dt}[F4] = \frac{d}{dt}[F4]_1 + \frac{d}{dt}[F4]_2 + \ldots + \frac{d}{dt}[F4]_6$$

$$\frac{d}{dt}[C1] = \frac{d}{dt}[C1]_1 + \frac{d}{dt}[C1]_2 + \ldots + \frac{d}{dt}[C1]_6$$

$$\frac{d}{dt}[C2] = \frac{d}{dt}[C2]_1 + \frac{d}{dt}[C2]_2 + \ldots + \frac{d}{dt}[C2]_6$$

which result in:

$$\frac{d}{dt}[F1] = k_a \cdot \left\{-2\cdot[F1]^2 - [F2]\cdot[F1] - [F3]\cdot[F1] - J\cdot[F1]\right\} + k_{d,f}\cdot\{2\cdot[F2] + 2\cdot[F3] + 2\cdot[F4]\} + k_{d,c}\cdot[C1]$$

$$\frac{d}{dt}[F2] = k_a \cdot \left\{[F1]^2 - [F2]\cdot[F1] - 2\cdot[F2]^2 - J_2\cdot[F2]\right\} + k_{d,c}\cdot\{-[F2] + 2\cdot[F3] + 2\cdot[F4]\} + 2\cdot k_{d,c}\cdot[C2]$$

$$\frac{d}{dt}[F3] = k_a \cdot \{[F2]\cdot[F1] - [F3]\cdot[F1]\} + k_{d,f}\cdot\{-2\cdot[F3] + 2\cdot[F4]\}$$

$$\frac{d}{dt}[F4] = k_a \cdot \{[F2]^2 + [F3]\cdot[F1]\} - 3\cdot k_{d,f}\cdot[F4]$$

$$\frac{d}{dt}[C1] = k_a \cdot J\cdot[F1] - k_{d,c}\cdot[C1]$$

$$\frac{d}{dt}[C2] = k_a \cdot J_2\cdot[F2] - 2\cdot k_{d,c}\cdot[C2]$$

Initially at t = 0, [F1] = $[F1]_0$ and other species are absent.

Nondimentionalization of ODEs

Nondimentionalization is performed by normalizing the concentrations with respect to $[F1]_0$. The normalized concentrations are denoted by a bar on top.

$$\overline{[F1]} = [F1]/[F1]_0$$

$$\overline{[F2]} = [F2]/[F1]_0$$

$$\overline{[F3]} = [F3]/[F1]_0$$

$$\overline{[F4]} = [F4]/[F1]_0$$

$$\overline{[C1]} = [C1]/[F1]_0$$

$$\overline{[C2]} = [C2]/[F1]_0$$

$$\bar{J} = J/[F1]_0$$

$$\overline{J_2} = J_2/[F1]_0$$

Final equations are then expressed as:

$$\frac{d}{dt}\overline{[F1]} = k_a \cdot [F1]_0 \cdot \left\{ -2\cdot\overline{[F1]}^2 - \overline{[F2]}\cdot\overline{[F1]} - \overline{[F3]}\cdot\overline{[F1]} - \bar{J}\cdot\overline{[F1]} \right\} + k_{d,f} \cdot \left\{ 2\cdot\overline{[F2]} + 2\cdot\overline{[F3]} + 2\cdot\overline{[F4]} \right\} + k_{d,c}\cdot\overline{[C1]}$$

$$\frac{d}{dt}\overline{[F2]} = k_a \cdot [F1]_0 \cdot \left\{ \overline{[F1]}^2 - \overline{[F2]}\cdot\overline{[F1]} - 2\cdot\overline{[F2]}^2 - \overline{J_2}\cdot\overline{[F2]} \right\} + k_{d,f} \cdot \left\{ -\overline{[F2]} + 2\cdot\overline{[F3]} + 2\cdot\overline{[F4]} \right\} + 2\cdot k_{d,c}\cdot\overline{[C2]}$$

$$\frac{d}{dt}\overline{[F3]} = k_a \cdot [F1]_0 \cdot \left\{ \overline{[F2]}\cdot\overline{[F1]} - \overline{[F3]}\cdot\overline{[F1]} \right\} + k_{d,f} \cdot \left\{ -2\cdot\overline{[F3]} + 2\cdot\overline{[F4]} \right\}$$

$$\frac{d}{dt}\overline{[F4]} = k_a \cdot [F1]_0 \cdot \{ \overline{[F2]}^2 + \overline{[F3]}\cdot\overline{[F1]} \} - 3\cdot k_{d,f}\cdot\overline{[F4]}$$

$$\frac{d}{dt}\overline{[C1]} = k_a \cdot [F1]_0 \cdot \bar{J}\cdot\overline{[F1]} - k_{d,c}\cdot\overline{[C1]}$$

$$\frac{d}{dt}\overline{[C2]} = k_a \cdot [F1]_0 \cdot \overline{J_2}\cdot\overline{[F2]} - 2\cdot k_{d,c}\cdot\overline{[C2]}$$

This ODE set can be numerically solved. The total dimensionless concentration of tiles is conserved to be 1 for this ODE set. Conversion from the nondimensionalized concentration to mass fraction (expressed in %) can be achieved by multiplication by $n\times100$ % (n=1 for *F1* and *C1*; n=2 for *F2*, and *C2*; etc.). Parameters (k_a, $\bar{J}$, $\overline{J_2}$ and k_d) are numerically fitted using fminsearch function in Matlab to minimize the error (i.e. least squares fitting) between ODE solution and counting statistics from AFM measurements.

S2. Detailed Calculation of Elastic Energy Barrier

Parameters and constants used in the mechanical analysis:

The following mechanical parameters are adapted from CanDo[6,7].

Torsional rigidity of a DNA double helix:	$T = 460$ pN·nm^2
Bending rigidity of a DNA double helix:	$B = 230$ pN·nm^2
Axial distance between base pairs in a DNA double helix:	$a = 0.34$ nm
Helical pitch of unstrained B form DNA double helix:	10.5 bp/turn
Torsional and bending rigidity of a single strand:	1/100 that of a double strand (nick factor 1/100)

Model Setup

Figure S2a shows the schematic of 16-bp double helix. Similar to CanDo, we simplify the DNA helix as a string of nodes connected by elastic beams as illustrated in Figure S2b. Base-pairs are treated as nodes (shown as balls), and phosphate bonds are abstracted as elastic beams (shown as rods). To facilitate analysis, the nodes are modeled as completely rigid, while the flexibility of a strand is completely attributed to the elastic beams.

In our analysis, three types of beams are relevant, which respectively represent: phosphate bond pairs, single phosphate bonds and crossover phosphate bonds. In double strand DNA, the two phosphate bonds connecting neighboring base-pairs are reinforced by the base-recognition. As a result, such phosphate bond pair is much stiffer than the single phosphate bond in single-stranded DNA or at the nick of a double-stranded DNA. To account for this effect, a phosphate bond pair in intact double helix DNA and a single phosphate bond at nick position are modeled as two different elastic beams whose stiffness is 100 times different.

Figure S2c shows the schematic of an antiparallel crossover, a critical structural element in most DNA origami designs. At crossover position, the crossover strands (red and purple) reverse their axial directions and participate in the formation of two neighboring double helices. Continuous base-pairing is disrupted for all of the four strands involved in the crossover. The two phosphate bonds that connect the two double helices do not reinforce each other. Therefore, their stiffness is expected to be in a similar order to that of the single phosphate bond at a nick position. We assume that each crossover phosphate bond is α times stiffer than a single phosphate bond.

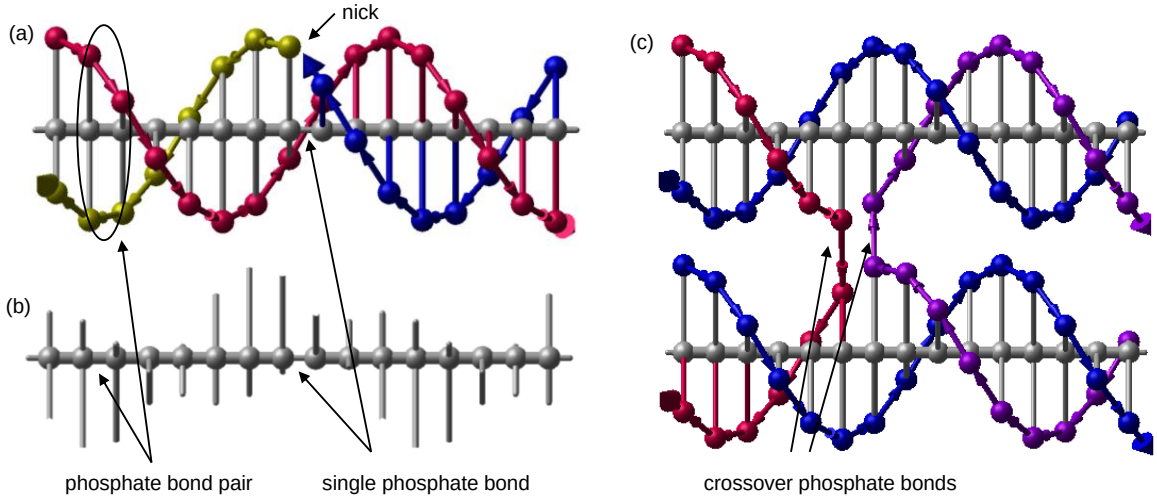

Figure S2: (a) Ball and stick model of a DNA double helix. (b) Node and beam abstraction of the DNA helix. (c) Ball and stick model of an antiparallel crossover. Black arrows point to the relevant bonds that are to be modeled as elastic beams in our mechanical model.

Two modes of deformation relevant in our analysis

1. Twisting of phosphate bond pair and single phosphate bond: The torsional spring constant for a phosphate bond pair is k1. k1 is the same as the torsional rigidity of a 1-base-long double stranded DNA:

$$k1 = \frac{T}{a} = 1.35\times10^{-18}\ \text{N}\cdot\text{m/rad} = 8.45\ \text{eV/rad}.$$

The spring constant of a single phosphate bond, k1′, is 1/100 of k1:

$$k1' = k1 / 100 = 8.45\times10^{-2}\ \text{eV/rad}.$$

2. Bending of crossover phosphate bond: The bending spring constant of one bond is denoted by k2. We assume that k2 is α times more rigid than a single phosphate bond. Therefore:

$$k2 = \alpha\frac{B}{100a} = \alpha\cdot4.22\times10^{-2}\ \text{eV/rad}.$$

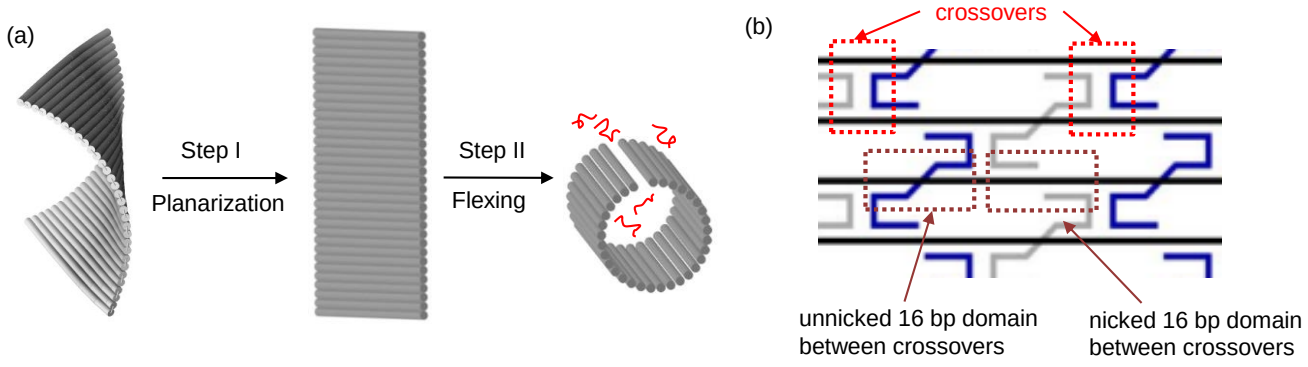

Figure S3: (a) Illustration of the conceptual two-step folding process. Step I eliminates the global twisting of the DNA tile. Step II flex the planar DNA sheet into circular conformation for the linkers to seal the two edges. (b) Diagram of folding path for a small segment of the origami tile. The relevant mechanical components are marked out in the diagram.

As discussed in the manuscript, the folding reconfiguration process can be conceptually divided into two steps. Step I forces the double helices into 10.66 bp/turn helical pitch, thereby planarizing the tile. Step II flex the planer tile into circular conformation by deforming the flexible components.

In **Step I**, the 16-bp domain between crossovers needs to be twisted into 10.66 bp/turn from 10.5 bp/turn. The twist angle is:

$$\Delta\theta = \left(\frac{360°}{10.66} - \frac{360°}{10.5}\right)\cdot16 = -8.23° = -0.144\ \text{rad}$$

For 16-bp helix between crossovers that does not contain any nicks, the equivalent spring constant is that of 15 phosphate bond pairs (k1) in serial. The elastic energy for forcing this domain is:

$$e_t = \frac{1}{2}\cdot\frac{k1}{15}\cdot\Delta\theta^2 = 5.84\times10^{-3}\ \text{eV}.$$

For 16-bp helix between crossovers that contain one nick, the equivalent spring constant is that of 14 phosphate bond pairs (k1) and 1 single phosphate bond ($k1' = \frac{k1}{100}$) in serial. The elastic energy for forcing this domain is:

$$e_t' = \frac{1}{2}\cdot\frac{1}{\frac{14}{k1}+\frac{100}{k1}}\cdot\Delta\theta^2 = 7.68\times10^{-4}\ \text{eV}.$$

N is used to denote the number of helices in a rectangle. As can be counted from Figure S4a, there are 6·(N-4) unnicked 16-bp domains and 6·(N-4) nicked 16-bp domains for a rectangle of N helices. (The upper 2 and lower 2 helices are incompletely base-paired. The long single stranded domain allows them to adapt to any helical pitch without considerable strain) The energy of **Step I** for 32-helice rectangle is:

$E_1 = 168e_t + 168e_t' = 1.110$ eV = 25.6 kcal/mol.

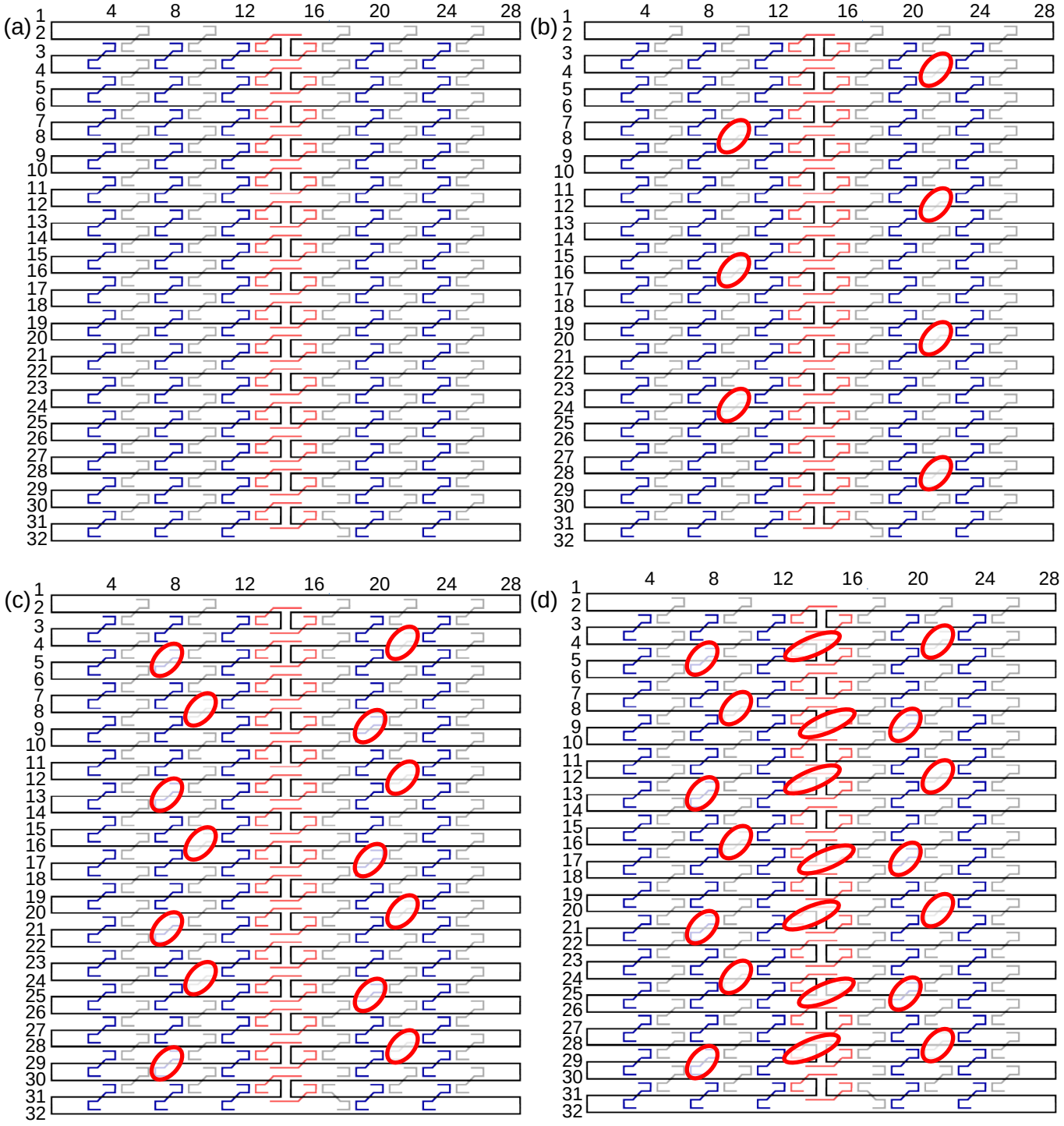

Figure S4: Schematic of origami folding path with missing staples marked in red circles. (a) Without any missing staples. (b) Missing 7 staples. (c) Missing 14 staples. (d) Missing 21 staples.

In **Step II**, the twisting flexibility of the 16-bp domain between opposite crossovers (Figure S5b) and the bending flexibility of crossover phosphate bonds (Figure S5c) enable the tile to flex into a circular conformation. We model the origami as a network of springs as illustrated in Figures S5d and S5e. Helices #1, 2, 31, and 32 are not fully hybridized. Although they may have considerable twisting flexibility, their twisting contributes little to the global bending because they are situated at the very ends of the origami tile. Therefore, helices #1 and 32 are completely excluded from the network, and the torsional flexibility of helices #2 and 31 is not considered in our analysis.

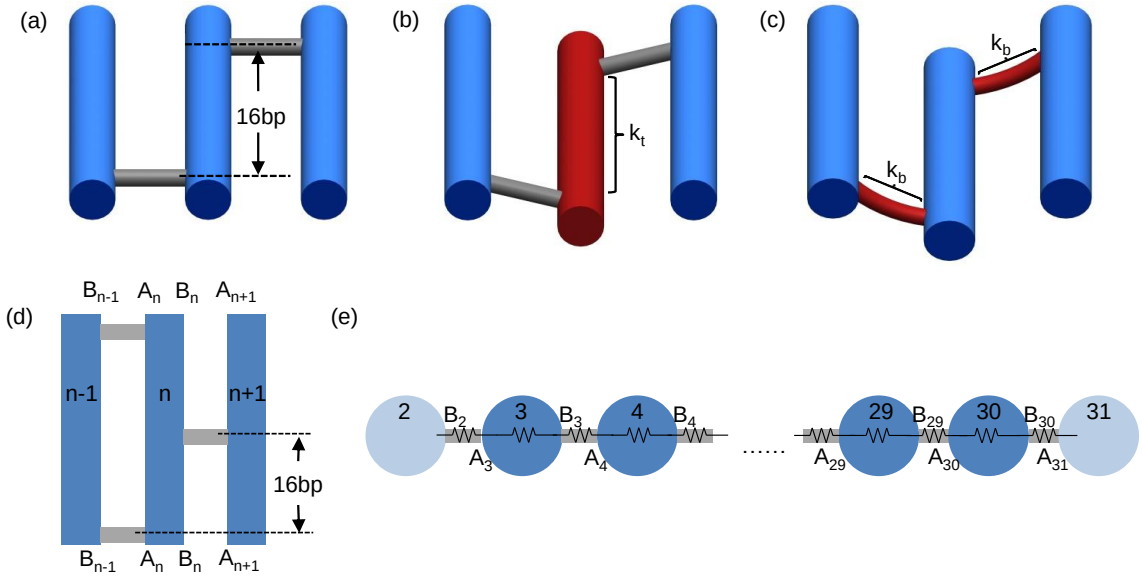

Figure S5: (a)-(c) Schematic of the deformation modes in a structural motif of DNA origami: the undeformed motif (a), twisting of the helix (b), and bending of crossovers (c). (d) Top view of the structural motif of DNA origami with the positions of each node marked. (e) Side view of the whole origami tile with the equivalent spring network superimposed. Blue color represents helices and gray color denotes crossovers. Red color highlights the deformed components.

From the complete folding diagram presented in Figure S4, we calculate the spring constant for each spring in the network shown in Figure S5e:

$k_b(B_2, A_3)$ denotes the collective bending spring constant of all the crossovers between helix #2 and #3. There are 12 crossover phosphate bonds from the staples and 2 such bonds from the scaffold. Since these bonds are in parallel[8], $k_b(B_2, A_3) = 14 \cdot k2$.

$k_t(A3, B3)$ denotes the torsional spring constant of helix #3. The helix has 5 unnicked 16-bp domains and 5 nicked 16-bp domains. These domains also function in parallel. From the analysis of E_1, we have already calculated that the spring constant for unnicked and nicked domain is $\frac{k1}{15}$ and $\frac{k1}{114}$, respectively. Therefore, $k_t(A3, B3) = 5 \cdot \frac{k1}{15} + 5 \cdot \frac{k1}{114} = 0.3772 \cdot k1$.

$k_b(B_3, A_4)$ consists of 10 crossover phosphate bonds from the staples. On the left and right edges of the origami, the scaffold forms two flexible loops that do not contribute significantly to mechanical rigidity. Therefore, $k_b(B3, A4) = 10 \cdot k_2$.

The folding path repeats itself every two rows. Therefore,

$k_b(B_{2n}, A_{2n+1}) = k_b(B_2, A_3)$ and $k_b(B_{2n+1}, A_{2n+2}) = k_b(B_3, A_4)$.

In addition, each helix contains the same number of unnicked and nicked 16-bp domains. Therefore,

$k_t(A_n, A_n) = k_t(A_3, A_3)$.

Overall, for a 224-bp wide, N-helices-high rectangular origami, we can summarize:

$k_t(A_n, B_n) = 0.3772 \cdot k1$ total number (N-4)

$k_b(B_{2m}, A_{2m+1}) = 14 \cdot k_2$ total number (N/2-1)

$k_b(B_{2m+1}, A_{2m+2}) = 10 \cdot k_2$ total number (N/2-2).

As shown in Figure S5e, these springs are in serial. Therefore, the effective spring constant of the spring network is

$$k_{eff} = \frac{1}{\frac{N-4}{0.3772 \cdot k1} + \frac{N/2-1}{14 \cdot k2} + \frac{N/2-2}{10 \cdot k2}}.$$

To achieve circular conformation, the total bending angle needs to reach 2π. Therefore,

$$E_2 = \frac{1}{2} k_{eff} (2\pi)^2.$$

The **final formula** for calculating the total elastic energy barrier is:

$$E_{elastic} = E_1 + E_2 = 6(N-4)(et + et') + \frac{1}{2} \cdot \frac{(2\pi^2)}{\frac{N-4}{0.3772 \cdot k1} + \frac{N/2-1}{14 \cdot k2} + \frac{N/2-2}{10 \cdot k2}}.$$

Determination of Crossover Rigidity

By varying the value of α, a series of $E_{elastic}$ can be calculated as a function of origami height. Figure S6 presents a few of such curves. Compared to Figure 9 in the main manuscript, α is changed in finer steps here. From our experimental observation,

$E_{elastic}$ (32-helix tile) > $E_{elastic}$ (12-helix tile) > $E_{elastic}$ (22-helix tile).

This inequality can be satisfied only when α is between 0.6 and 1.2. For simplicity, we choose α=1. Consequently,

E_2 = 0.293 eV = 6.7 kcal/mol.

$E_{elastic}$ (32-helix) = $E_1 + E_2$ = 1.403 eV = 32.3 kcal/mol, which is very close to experimentally derived value.

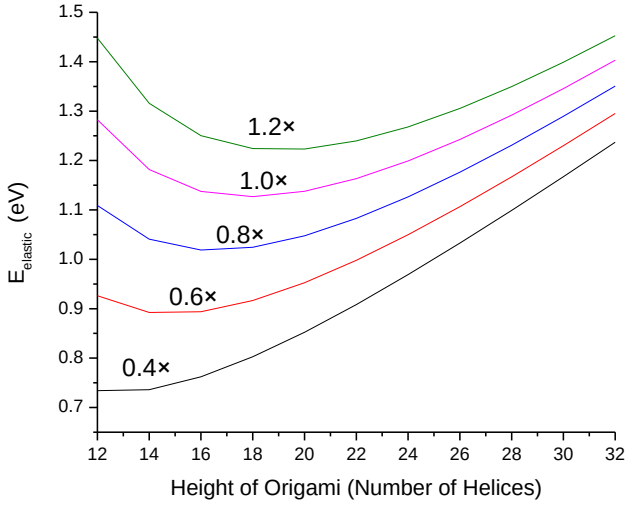

Figure S6: Calculated elastic energy barrier as a function of origami height for different crossover rigidity. The bending rigidity of crossovers is varied from 0.4 to 1.2 times the bending rigidity of a 1-base-long single-stranded DNA, as marked near each curve.

Calculation of elastic energy for an origami rectangle with 7 missing staples:

For the 32-helix rectangle with 7 missing staples (Figure S4b), 7 un-nicked 16-bp domains and 14 nicked 16-bp domains will be disrupted.

For **step I,** there is no need to force the disrupted domains into 10.66 bp/turn. Therefore, E_1 change by:

$\Delta E1 = -7e_t - 7e_t' = -5.16\times10^{-2}$ eV = -1.19 kcal/mol.

For **Step II**, the disrupted 16-bp domains no longer produce torques upon twisting.

7 helices (#4, 8, 12, ..., 28) have one unnicked domain disrupted. Consequently, k_t(An, Bn) is reduced to

$$4\cdot\frac{k1}{15}+5\cdot\frac{k1}{114}=0.3105\cdot k1.$$

14 helices (#3,7, ..., 27 and #5, 9, ..., 29) have one nicked domain disrupted. Therefore, k_t(An, Bn) decreases to

$$5\cdot\frac{k1}{15}+4\cdot\frac{k1}{114}=0.3642\cdot k1.$$

7 helices are not affected, k_t(An, Bn) remains $0.3772\cdot k1$.

The missing staples also reduce the number of crossover phosphate bonds.

7 even to odd inter-helix joints lose one bond. Consequently $k_b(B_{2m}, A_{2m+1})$ changes into $13\cdot k2$; (m=2, 4, 6, ..., 14).

7 odd to even inter-helix joints lose one bond. Consequently $k_b(B_{2m+1}, A_{2m+2})$ changes into $9\cdot k2$; (m=1, 3, 5, ..., 13).

The rest of the 8 even to odd joints and 7 odd to even joints are not affected.

Consider all these decreases in spring constant, E_2 is recalculated to be:

$$E_2' = \frac{1}{2}\cdot\frac{(2\pi^2)}{\frac{7}{0.3772\cdot k1}+\frac{7}{0.3105\cdot k1}+\frac{14}{0.3642\cdot k1}+\frac{8}{14\cdot k2}+\frac{7}{13\cdot k2}+\frac{7}{10\cdot k2}+\frac{7}{9\cdot k2}} = 0.2791 \text{ eV}$$

Originally,

$$E_2=\frac{1}{2}\cdot\frac{(2\pi^2)}{\frac{28}{0.3772\cdot k1}+\frac{15}{14\cdot k2}+\frac{14}{10\cdot k2}} = 0.2931 \text{ eV}.$$

Finally, the change of E_2 becomes: $\Delta E_2 = E_2' - E_2 = -1.40\times10^{-2}$ eV = -0.32 kcal/mol.

The change in the total energy barrier in the two steps is:

$\Delta E_{elastic}=\Delta E_1+\Delta E_2 = 6.56\times10^{-2}$ eV = -1.51 kcal/mol.

The effect of missing staples was experimentally tested at 40 °C. At this temperature, the thermal energy is:

kT = 0.622 kcal/mol.

The j-factor is expected to increase $\exp(-\Delta E_{elastic} / kT) = 11$ times, while the experimental increase was 12. Since the increase depend exponentially on our predicted energy barrier, the prediction value is reasonably good.

Side note

Our simple spring network model predicts the energy barrier with reasonable accuracy. It should be noted that the model is applicable under the conditions described in this work. Due to its simplicity, our model works best for highly regular origami. It also requires the origami tile to be nearly intact (i.e. the number of missing staples is small). When too many staples are eliminated, the structural effect becomes too complex to predict. For complex geometry, computer-based finite element analysis tools such as CanDo may be necessary.

Of considerable utility of our mechanical model is that it facilitates the estimation of crossover rigidity. CanDo treats crossovers as rigid constraints. This treatment works well for predicting the dynamic behavior of multilayered structure and the equilibrium structure of origami in general. In a multilayer structure, the crossover bending degree-of-freedom is largely prohibited. Moreover, the crossover bending flexibility does not affect equilibrium structure. For these reasons, CanDo has been highly successful in its prediction even though it does not consider the significant bending flexibility of crossovers. The estimation of this work should be valuable for predicting the dynamic behavior of more flexible origami structures.

S3. Effect of Model Fitting Constraints

Four different set of constraints are used in fitting the model solution to experimental mass fraction data. The dissociation rate constant for flat species, $k_{d,f}$ can be assigned to equal $k_{d,c}$ or 0 ($0 \le k_{d,f} \le k_{d,c}$); the j-factor for dimers, J_2 can be assigned to equal J or assume an independent value to be extracted by residual minimization. In combination, four constrain conditions are possible. All four conditions yield generally satisfactory agreement between experimental data and model solution. The most pronounced difference occurs for the (45 °C, 4.2 nM) and (40 °C, 4.2 nM) conditions. Fitting results are compared in Figures S7 and S8 below.

Compare the panels in Figure S7 horizontally, it can be seen that for panel a and c, where J_2 is not independently optimized, the ratio between *F2* and *C2* species is off. -(However, as shown in Figure S9, the extracted values of other kinetic parameters are hardly affected). Compared vertically, it can be seen that when $k_{d,f} = k_{d,c}$ (panel c and d), the *F2* species increases more rapidly at the beginning and decreases more noticeably at a later stage. Experimentally, the increase of *F2* was not as fast, nor was such a distinctive decrease observed. Therefore, we conclude that the $k_{d,f} = 0$ condition gives better fit and is closer to the real situation. Figure S8 compares the effect of $k_{d,f}$ further. Again, the $k_{d,f} = 0$ condition fits the evolution of *F2* fraction better.

Figure S9 compares the extracted kinetic parameters under different fitting conditions. The use of independent J_2 has little effect on the extraction of other parameters. Dictating that $k_{d,f} = k_{d,c}$ will result in larger k_a and smaller J. This interdependence between parameters can be qualitatively understood. The low percentage of flat oligomers (e.g. *F2*) can result from both large J (rapid consumption of reactant monomer by cyclization reaction) or large $k_{d,f}$ (rapid degradation of formed oligomers). When $k_{d,f}$ is increased (from 0), J has to be decreased to keep the overall effect unchanged. Due to decreased J, k_a needs to be increased to keep the cyclization rate $J \cdot k_a$ at the same level. Depending on the choice of $k_{d,f}$, the absolute value for J and k_a may have moderate scaling up to 3-fold. However, the trends for k_a and J are not significantly dependent on the fitting constraints. Since the trend is all we need to extract activation energy for further mechanical analysis, the choice of fitting condition does not alter the conclusion of our mechanical analysis.

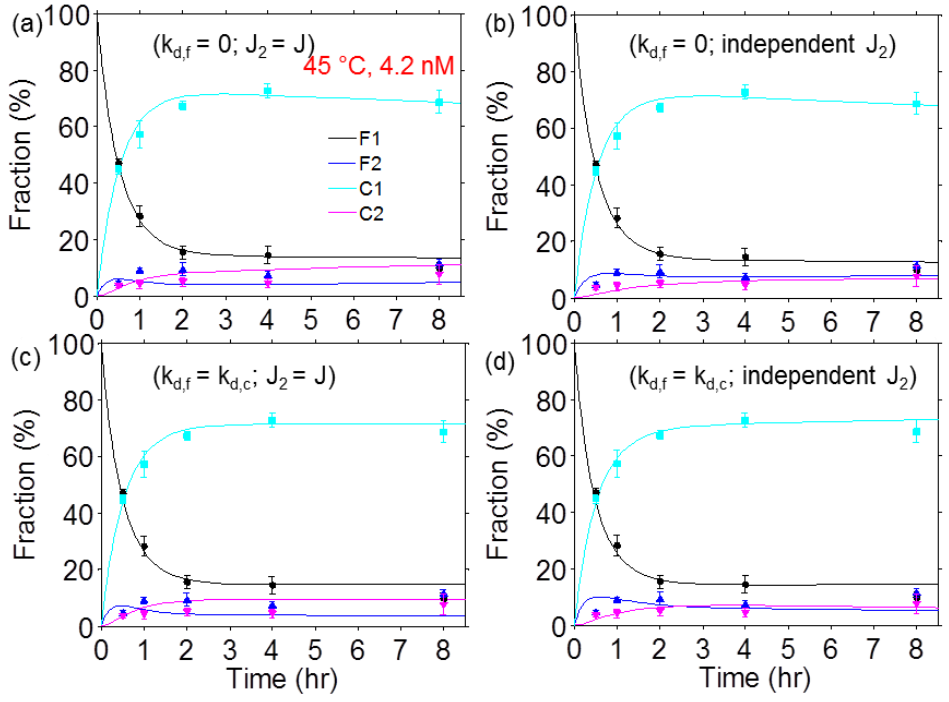

Figure S7: Experimental and model simulated species fraction evolution from 4.2 nM tile concentration at 45 °C. Four simulation conditions are examined and compared: (a) $k_{d,f} = 0$; $J_2 = J$, (b) $k_{d,f} = 0$; independent J_2, (c) $k_{d,f} = k_{d,c}$; $J_2 = J$, (d) $k_{d,f} = k_{d,c}$; independent J_2.

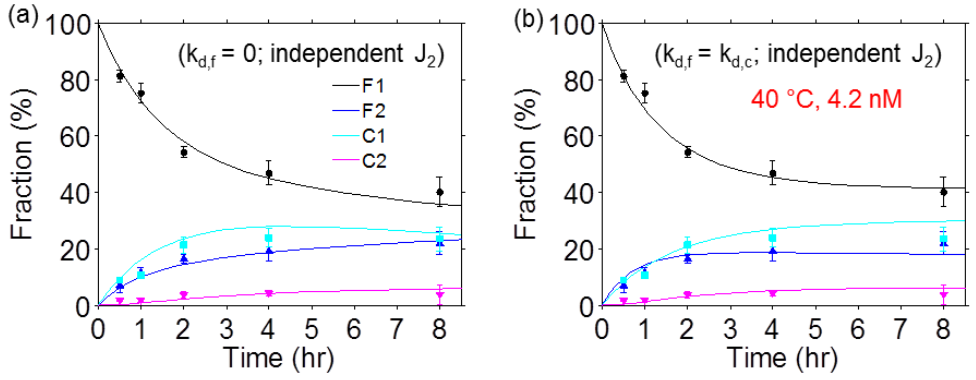

Figure S8: Experimental and model simulated species fraction evolution from 4.2 nM tile concentration at 40 °C. Two simulation conditions are examined and compared: (a) $k_{d,f} = 0$; independent J_2; (b) $k_{d,f} = k_{d,c}$; independent J_2.

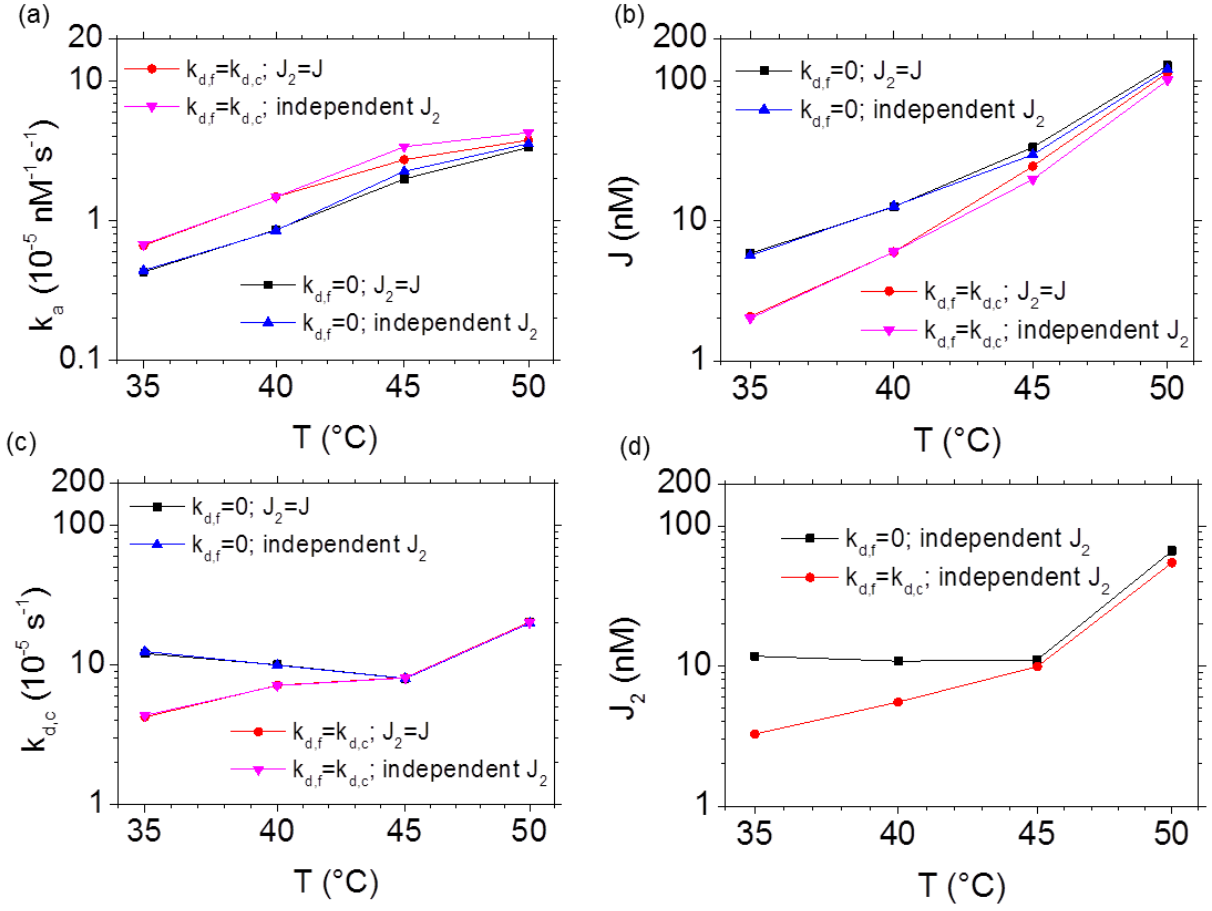

Figure S9: Comparison of extracted kinetic parameters for different fitting conditions. (a) Association constant (k_a). (b) J, the j-factor of monomer tiles. (c) Dissociation constant ($k_{d,c}$) for cyclized species. (d) J_2, the j-factor of dimers when it is individually optimized. The vertical scales are all set to 200-fold for easy visualization of relative changes.

S4. Uncertainty Analysis

The fraction of origami species are statistically estimated in this study. The estimation is subject to fundamental statistical fluctuations. Such fluctuation can be estimated in theory. Beside the statistical fluctuation, there are other sources of uncertainty such as errors in identifying species and the possible variation caused by the deposition process. The overall uncertainty from all sources is estimated by weighted standard deviation between multiple statistical results each derived from one AFM image. Calculation methods are presented below.

Estimation of statistical fluctuation:

The deposition of origami structures on mica substrate is a stochastic process. At a given deposition condition (e.g. origami concentration, surface affinity, and deposition time), the number of one species on a 5-μm × 5-μm area is expected to fluctuate around an expectation value. If the expected occurrence of one species is $\overline{N_i}$, it is reasonable to assume that the standard deviation is $\sqrt{\overline{N_i}}$ [9]. Here we simply denote the counted occurrence of the species *Fn* by its name, *Fn*, and denote its mass fraction by [*Fn*]. The total number of tiles counted for one measurement is denoted by N. Then

$$N = F1 + 2\cdot F2 + 3\cdot F3 + 4\cdot F4 + C1 + 2\cdot C2$$

$[Fn] = \frac{n \cdot Fn}{N}$, which is a function of the raw counted occurrence (i.e. *F1, F2, F3, F4, C1,* and *C2*).

Take flat monomer, *F1,* as an example:

$$[F1] = \frac{F1}{N}$$

$$d[F1] = \frac{\partial[F1]}{\partial F1}\cdot dF1 + \frac{\partial[F1]}{\partial F2}\cdot dF2 + \frac{\partial[F1]}{\partial F3}\cdot dF3 + \frac{\partial[F1]}{\partial F4}\cdot dF4 + \frac{\partial[F1]}{\partial C1}\cdot dC1 + \frac{\partial[F1]}{\partial C2}\cdot dC2$$

$$= (1-[F1])\cdot\frac{1}{N}\cdot dF1 - [F1]\cdot\frac{2}{N}\cdot dF2 - [F1]\cdot\frac{3}{N}\cdot dF3 - [F1]\cdot\frac{4}{N}\cdot dF4 - [F1]\cdot\frac{1}{N}\cdot dC1 - [F1]\cdot\frac{2}{N}\cdot dC2$$

According to theories of uncertainty analysis[10], assuming independent fluctuation of the raw counting results, the uncertainty can be expressed as:

$$\Delta[F1] = \sqrt{(\frac{\partial[F1]}{\partial F1})^2\cdot\Delta F1^2 + (\frac{\partial[F1]}{\partial F2})^2\cdot\Delta F2^2 + (\frac{\partial[F1]}{\partial F3})^2\cdot\Delta F3^2 + (\frac{\partial[F1]}{\partial F4})^2\cdot\Delta F4^2 + (\frac{\partial[F1]}{\partial C1})^2\cdot\Delta C1^2 + (\frac{\partial[F1]}{\partial C2})^2\cdot\Delta C2^2}\ .$$

Here we use the actual counted occurrence number as an estimation of occurrence expectation. Therefore,

$$\Delta Fi = \sqrt{Fi}$$

Finally, it can be derived that:

$$\Delta[F1] = \frac{1}{N}\sqrt{(1-[F1])^2 F1 + [F1]^2\cdot(4\cdot F2 + 9\cdot F3 + 16\cdot F4 + C1 + 4\cdot C2)}$$

$$= \frac{1}{\sqrt{N}}\sqrt{(1-[F1])^2[F1] + [F1]^2\cdot(2\cdot[F2] + 3\cdot[F3] + 4\cdot[F4] + [C1] + 2\cdot[C2])} \qquad \text{(E1).}$$

Similarly,

$$\Delta[F2] = \frac{1}{\sqrt{N}}\sqrt{(1-[F2])^2\cdot 2\cdot[F2] + [F2]^2\cdot([F1] + 3\cdot[F3] + 4\cdot[F4] + [C1] + 2\cdot[C2])} \qquad \text{(E2),}$$

$$\Delta[C1] = \frac{1}{\sqrt{N}}\sqrt{(1-[C1])^2[C1] + [C1]^2\cdot([F1] + 2\cdot[F2] + 3\cdot[F3] + 4\cdot[F4] + 2\cdot[C2])} \qquad \text{(E3), and}$$

$$\Delta[C2] = \frac{1}{\sqrt{N}}\sqrt{(1-[C2])^2 \cdot 2 \cdot [C2] + [C2]^2 \cdot ([F1] + 2 \cdot [F2] + 3 \cdot [F3] + 4 \cdot [F4] + [C1])} \qquad \text{(E4)}.$$

Equations E1 through E4 estimates the uncertainty caused by statistical fluctuation when a certain number of tiles are counted.

Experimental estimation:

Experimentally, each composition measurement is based on three or more 5-μm × 5-μm AFM images. Individual counting and statistical analysis is performed for each image and the calculated species mass fraction can be compared between images to assess the variation. When there are m images, for each species X, there will be m calculated values denoted by $[X]_1$, $[X]_2$, ... ,$[X]_m$, the weighted standard deviation[11] for [X] is calculated by

$$\Delta[X] = \sqrt{\frac{\sum_{i=1}^{m} w_i \cdot ([X]_i - \overline{[X]})^2}{(m-1)\overline{w}}}$$

where the weight w_i associated with $[X]_i$ is the number of tiles that the corresponding image contains. $\overline{w}$ is the average number of tiles that one image contains.

$$\overline{w} = \frac{\sum_{i=1}^{m} w_i}{m}$$

$\overline{[X]}$ is the weighted average[11] of the measurement result, given by:

$$\overline{[X]} = \frac{\sum_{i=1}^{m} w_i \cdot [X]_i}{\sum_{i=1}^{m} w_i}$$

Ideally, the standard deviation between images should only result from the statistical fluctuation discussed above. Due to other sources of uncertainty, the calculated standard deviation in our experiment is typically 1~3 times larger than predicted statistical fluctuation. In the rare cases where the calculated standard deviation is smaller than theoretical statistical fluctuation, the later is used as the overall uncertainty.

The raw counting result, averaged fraction value and uncertainty are listed below in Table S1a-h. Separate uncertainty values are listed below the weighted average. Et denote theoretically predicted statistical fluctuation and Ee denote weighted standard deviation. Since the standard deviation typically does not exceed the theoretical statistical fluctuation by 3 times, the statistical relevance of our data is confirmed.

Table S1: Raw counting results and calculated average species fraction with uncertainty. Et denotes theoretically estimated uncertainty and Ee denote experimentally estimated uncertainty.

Table S1a. Counting and statistical result: 35 °C, 4.2 nM case										Incubation
Counting Result: Occurrence						Statistical Result: Mass Fraction (%)				
F1	F2	C1	C2	F3	F4	F1	F2	C1	C2	Time (hr)
258	3	8	0	0	0	**94.2±1.1**	**4.0±1.6**	**1.9±1.0**	**0.0±0.0**	0.5
363	10	4	0	0	0	Et: ±1.1	Et: ±1.0	Et: ±0.5	Et: ±0.0	
140	3	3	0	0	0	Ee: ±0.6	Ee: ±1.6	Ee: ±1.0	Ee: ±0.0	
127	9	7	1	0	0	**87.0±4.4**	**9.4±2.3**	**3.1±1.4**	**0.4±0.8**	1
152	6	3	0	0	0	Et: ±2.0	Et: ±1.9	Et: ±0.8	Et: ±0.4	
110	6	4	0	0	0	Ee: ±4.4	Ee: ±2.3	Ee: ±1.4	Ee: ±0.8	
385	28	14	1	1	0	**80.2±3.9**	**13.7±2.5**	**3.8±0.9**	**0.9±0.6**	2
436	34	18	3	1	1	Et: ±1.2	Et: ±1.2	Et: ±0.5	Et: ±0.3	
402	44	25	2	3	1	Ee: ±3.9	Ee: ±2.5	Ee: ±0.9	Ee: ±0.6	
82	14	5	0	2	0	**67.7±2.5**	**19.8±2.9**	**6.1±1.8**	**3.0±2.0**	4
73	11	9	2	0	1	Et: ±2.5	Et: ±2.5	Et: ±1.1	Et: ±1.1	
73	11	8	2	0	0	Ee: ±1.8	Ee: ±2.9	Ee: ±1.8	Ee: ±2.0	
93	11	7	3	2	0					
85	15	8	2	1	0	**61.1±3.5**	**25.8±2.8**	**7.5±1.8**	**2.4±1.0**	8
85	18	9	2	3	1	Et: ±2.6	Et: ±2.6	Et: ±1.2	Et: ±1.0	
133	31	20	2	0	0	Ee: ±3.5	Ee: ±2.8	Ee: ±1.8	Ee: ±0.7	
Table S1b. Counting and statistical result: 35 °C, 1.3 nM case										Incubation
Counting Result: Occurrence						Statistical Result: Mass Fraction (%)				
F1	F2	C1	C2	F3	F4	F1	F2	C1	C2	Time (hr)
85	2	1	0	0	0	**93.6±3.3**	**4.0±1.6**	**1.7±1.6**	**0.7±0.9**	0.5
118	3	4	1	0	0	Et: ±1.8	Et: ±1.6	Et: ±0.7	Et: ±0.7	
75	1	0	0	0	0	Ee: ±3.3	Ee: ±1.0	Ee: ±1.6	Ee: ±0.9	
190	4	8	0	0	0	**91.4±1.4**	**3.7±1.1**	**4.6±1.2**	**0.3±0.5**	1
222	4	10	1	0	0	Et: ±1.4	Et: ±1.1	Et: ±0.9	Et: ±0.3	
127	3	9	0	0	0	Ee: ±1.3	Ee: ±0.5	Ee: ±1.2	Ee: ±0.5	
232	5	12	1	1	0	**89.5±3.9**	**4.6±1.1**	**4.2±2.0**	**0.9±0.8**	2
215	7	14	2	1	0	Et: ±1.4	Et: ±1.1	Et: ±0.8	Et: ±0.5	
178	4	3	0	0	0	Ee: ±3.9	Ee: ±0.9	Ee: ±2.0	Ee: ±0.8	
71	3	7	2	0	0	**82.0±3.5**	**7.7±2.6**	**8.8±2.5**	**1.4±2.4**	4
54	4	6	0	0	0	Et: ±2.7	Et: ±2.2	Et: ±1.7	Et: ±1.0	
56	2	4	0	0	0	Ee: ±3.5	Ee: ±2.6	Ee: ±2.5	Ee: ±2.4	
52	2	8	0	0	0					
167	20	20	2	2	0	**73.7±3.3**	**13.8±3.3**	**9.0±1.1**	**1.5±0.7**	8
160	15	18	2	0	1	Et: ±2.0	Et: ±1.8	Et: ±1.1	Et: ±0.7	
164	11	22	1	1	0	Ee: ±3.3	Ee: ±3.3	Ee: ±1.1	Ee: ±0.5	

Table S1c. Counting and statistical result: 40 °C, 4.2 nM case										Incubation
Counting Result: Occurrence						Statistical Result: Mass Fraction (%)				
F1	F2	C1	C2	F3	F4	F1	F2	C1	C2	Time (hr)
314	18	36	3	0	0	**81.4±2.2**	**7.1±2.5**	**9.0±0.8**	**1.9±0.6**	0.5
314	8	34	5	0	0	Et: ±1.3	Et: ±1.1	Et: ±0.8	Et: ±0.6	
310	15	34	3	2	0	Ee: ±2.2	Ee: ±2.5	Ee: ±0.2	Ee: ±0.6	
318	23	46	2	1	0	**75.3±3.4**	**11.6±1.7**	**10.7±1.3**	**1.7±0.7**	1
280	27	46	4	1	0	Et: ±1.4	Et: ±1.2	Et: ±0.8	Et: ±0.5	
312	23	43	5	1	0	Ee: ±3.4	Ee: ±1.7	Ee: ±1.3	Ee: ±0.7	
124	7	12	1	0	0					
129	20	58	3	2	0	**54.4±1.9**	**16.4±1.7**	**21.3±3.0**	**3.7±1.2**	2
180	26	58	8	3	1	Et: ±1.8	Et: ±1.7	Et: ±1.4	Et: ±0.9	
187	29	78	6	1	4	Ee: ±1.9	Ee: ±0.2	Ee: ±3.0	Ee: ±1.2	
162	28	96	7	4	5	**46.9±4.3**	**19.3±3.4**	**24.0±3.3**	**4.3±0.9**	4
150	35	84	9	2	3	Et: ±1.7	Et: ±1.7	Et: ±1.4	Et: ±0.9	
165	35	64	6	2	0	Ee: ±4.3	Ee: ±3.4	Ee: ±3.3	Ee: ±0.8	
41	10	21	0	1	1	**40.1±5.2**	**22.1±4.1**	**23.6±4.3**	**3.8±3.6**	8
34	12	25	2	4	1	Et: ±2.4	Et: ±2.5	Et: ±2.0	Et: ±1.2	
34	12	16	3	2	0	Ee: ±5.2	Ee: ±4.1	Ee: ±4.3	Ee: ±3.6	
42	9	23	4	3	2					
38	9	26	0	1	0					

Table S1d. Counting and statistical result: 40 °C, 1.3 nM case										Incubation
Counting Result: Occurrence						Statistical Result: Mass Fraction (%)				
F1	F2	C1	C2	F3	F4	F1	F2	C1	C2	Time (hr)
404	9	48	2	0	0	**85.3±1.2**	**3.8±1.8**	**10.4±1.4**	**0.5±0.4**	0.5
430	12	50	1	0	0	Et: ±1.2	Et: ±0.8	Et: ±0.9	Et: ±0.3	
109	0	17	0	0	0	Ee: ±0.6	Ee: ±1.8	Ee: ±1.4	Ee: ±0.4	
358	7	88	3	0	0	**76.9±1.3**	**3.5±0.7**	**18.6±1.1**	**0.8±0.8**	1
352	9	83	0	0	0	Et: ±1.3	Et: ±0.7	Et: ±1.1	Et: ±0.4	
223	5	55	2	1	0	Ee: ±1.0	Ee: ±0.5	Ee: ±0.3	Ee: ±0.8	
72	1	30	1	1	0	**67.3±2.6**	**3.3±1.3**	**27.5±2.8**	**1.1±1.1**	2
83	2	29	1	0	0	Et: ±2.5	Et: ±1.3	Et: ±2.3	Et: ±0.8	
92	3	42	0	0	0	Ee: ±2.6	Ee: ±1.2	Ee: ±2.8	Ee: ±1.1	
676	50	337	21	0	0	**55.3±3.8**	**10.0±2.3**	**30.3±2.4**	**3.1±0.7**	4
602	69	351	16	6	4	Et: ±1.1	Et: ±0.8	Et: ±0.9	Et: ±0.5	
116	7	77	2	0	0	Ee: ±3.8	Ee: ±2.3	Ee: ±2.4	Ee: ±0.7	
106	15	80	1	1	0	**46.9±5.3**	**12.1±1.7**	**36.8±4.1**	**2.4±1.3**	8
108	13	68	3	0	0	Et: ±2.0	Et: ±1.7	Et: ±1.9	Et: ±0.8	
96	12	95	4	3	0	Ee: ±5.3	Ee: ±1.7	Ee: ±4.1	Ee: ±1.3	

Table S1e. Counting and statistical result: 45 °C, 4.2 nM case										Incubation
Counting Result: Occurrence						Statistical Result: Mass Fraction (%)				
F1	F2	C1	C2	F3	F4	F1	F2	C1	C2	Time (hr)
285	13	260	12	0	0	**47.0±1.5**	**4.6±0.8**	**44.8±1.5**	**3.6±0.7**	0.5
272	14	259	9	0	0	Et: ±1.4	Et: ±0.8	Et: ±1.4	Et: ±0.7	
118	6	125	5	0	0	Ee: ±1.5	Ee: ±0.3	Ee: ±1.5	Ee: ±0.5	
140	21	243	9	0	0	**28.3±3.5**	**9.0±1.1**	**57.4±4.7**	**4.2±1.4**	1
194	31	474	12	4	1	Et: ±1.1	Et: ±1.0	Et: ±1.3	Et: ±0.7	
142	24	250	14	1	0	Ee: ±3.5	Ee: ±1.1	Ee: ±4.7	Ee: ±1.4	
53	14	266	8	5	2	**15.5±2.4**	**9.3±2.3**	**67.4±1.5**	**5.0±1.5**	2
57	23	260	8	3	0	Et: ±1.1	Et: ±1.2	Et: ±1.5	Et: ±0.9	
70	17	254	13	0	0	Ee: ±2.4	Ee: ±2.3	Ee: ±1.4	Ee: ±1.5	
39	14	258	5	1	1	**14.6±3.0**	**7.5±1.2**	**72.7±2.5**	**4.5±1.5**	4
49	11	220	9	0	0	Et: ±1.2	Et: ±1.2	Et: ±1.7	Et: ±0.9	
49	10	205	7	0	0	Ee: ±3.0	Ee: ±0.7	Ee: ±2.5	Ee: ±1.5	
30	23	245	22	4	1	**9.8±1.9**	**11.4±1.3**	**68.7±4.0**	**7.7±3.6**	8
36	20	245	11	1	0	Et: ±0.9	Et: ±1.3	Et: ±1.7	Et: ±1.1	
39	18	244	8	2	0	Ee: ±1.9	Ee: ±0.8	Ee: ±4.0	Ee: ±3.6	

Table S1f. Counting and statistical result: 45 °C, 1.3 nM case										Incubation
Counting Result: Occurrence						Statistical Result: Mass Fraction (%)				
F1	F2	C1	C2	F3	F4	F1	F2	C1	C2	Time (hr)
81	5	95	2	0	0	**44.4±2.2**	**1.8±3.1**	**51.6±3.1**	**2.2±1.3**	0.5
77	0	81	3	0	0	Et: ±2.2	Et: ±0.8	Et: ±2.2	Et: ±0.9	
83	0	104	1	0	0	Ee: ±2.2	Ee: ±3.1	Ee: ±3.1	Ee: ±1.3	
162	13	351	5	0	0	**30.9±1.4**	**4.3±1.0**	**62.6±1.2**	**2.2±0.5**	1
185	9	356	6	0	0	Et: ±1.1	Et: ±0.7	Et: ±1.2	Et: ±0.5	
181	15	363	8	0	0	Ee: ±1.4	Ee: ±1.0	Ee: ±1.2	Ee: ±0.5	
81	3	259	5	0	0	**18.5±4.7**	**3.2±1.9**	**75.5±4.5**	**2.5±0.7**	2
49	5	290	4	1	0	Et: ±1.2	Et: ±0.8	Et: ±1.4	Et: ±0.7	
65	9	245	4	0	0	Ee: ±4.7	Ee: ±1.9	Ee: ±4.5	Ee: ±0.3	
45	4	252	3	1	0	**14.0±3.8**	**2.2±0.7**	**80.5±1.4**	**2.7±1.6**	4
48	2	212	2	0	0	Et: ±1.2	Et: ±0.7	Et: ±1.4	Et: ±0.8	
32	4	257	7	1	0	Ee: ±3.8	Ee: ±0.6	Ee: ±1.4	Ee: ±1.6	
45	3	231	4	1	0	**14.5±2.7**	**2.5±0.7**	**80.9±3.4**	**1.8±0.8**	8
74	7	367	3	0	0	Et: ±1.1	Et: ±0.7	Et: ±1.3	Et: ±0.6	
29	3	230	2	0	0	Ee: ±2.7	Ee: ±0.6	Ee: ±3.4	Ee: ±0.8	

Table S1g. Counting and statistical result: 50 °C, 4.2 nM case										Incubation
Counting Result: Occurrence						Statistical Result: Mass Fraction (%)				
F1	F2	C1	C2	F3	F4	F1	F2	C1	C2	Time (hr)
74	0	247	2	0	0	**22.9±3.0**	**0.8±0.8**	**74.7±2.5**	**1.6±1.3**	1/6
95	3	265	1	0	0	Et: ±1.3	Et: ±0.4	Et: ±1.4	Et: ±0.5	
65	1	251	5	0	0	Ee: ±3.0	Ee: ±0.8	Ee: ±2.5	Ee: ±1.3	
113	7	809	7	0	0	**10.8±1.5**	**1.4±0.4**	**86.0±1.2**	**1.8±0.7**	1/3
41	2	389	6	0	0	Et: ±0.8	Et: ±0.4	Et: ±0.9	Et: ±0.4	
31	3	273	2	0	0	Ee: ±1.5	Ee: ±0.4	Ee: ±1.2	Ee: ±0.7	
22	2	222	3	0	0	**8.4±1.1**	**1.8±0.9**	**87.7±1.4**	**2.1±0.8**	0.5
32	3	335	4	0	0	Et: ±1.1	Et: ±0.7	Et: ±1.4	Et: ±0.8	
3	1	37	0	0	0	Ee: ±0.4	Ee: ±0.9	Ee: ±0.3	Ee: ±0.7	
34	2	367	7	0	0	**8.6±1.3**	**0.8±0.3**	**88.1±0.9**	**2.5±0.7**	1
45	1	384	4	0	0	Et: ±0.7	Et: ±0.3	Et: ±0.9	Et: ±0.6	
56	3	632	9	0	0	Ee: ±1.3	Ee: ±0.2	Ee: ±0.8	Ee: ±0.7	
42	7	651	6	0	0	**5.9±0.6**	**1.4±0.7**	**89.5±1.2**	**3.3±1.8**	2
43	3	644	17	0	0	Et: ±0.6	Et: ±0.4	Et: ±0.9	Et: ±0.6	
9	1	132	3	0	0	Ee: ±0.1	Ee: ±0.7	Ee: ±1.2	Ee: ±1.8	

Table S1h. Counting and statistical result: 50 °C, 1.3 nM case										Incubation
Counting Result: Occurrence						Statistical Result: Mass Fraction (%)				
F1	F2	C1	C2	F3	F4	F1	F2	C1	C2	Time (hr)
76	0	184	2	0	0	**24.7±3.4**	**0.2±0.4**	**74.1±3.6**	**0.9±0.5**	1/6
75	0	234	1	0	0	Et: ±1.5	Et: ±0.2	Et: ±1.5	Et: ±0.4	
68	1	238	1	0	0	Ee: ±3.4	Ee: ±0.4	Ee: ±3.6	Ee: ±0.5	
79	4	480	3	0	0	**13.1±1.1**	**1.1±0.6**	**84.5±0.9**	**1.1±0.4**	1/3
61	4	442	3	0	0	Et: ±0.8	Et: ±0.4	Et: ±0.9	Et: ±0.4	
72	1	450	3	1	0	Ee: ±1.1	Ee: ±0.6	Ee: ±0.9	Ee: ±0.1	
26	0	268	2	0	0	**7.6±1.2**	**0.0±0.0**	**90.8±1.1**	**1.6±1.0**	0.5
23	0	302	2	0	0	Et: ±1.0	Et: ±0.0	Et: ±1.1	Et: ±0.7	
7	0	99	2	0	0	Ee: ±1.2	Ee: ±0.0	Ee: ±1.1	Ee: ±1.0	
16	1	206	0	0	0	**5.8±1.3**	**1.0±0.6**	**91.2±1.3**	**2.0±2.1**	1
13	1	237	5	0	0	Et: ±1.0	Et: ±0.6	Et: ±1.3	Et: ±0.8	
5	1	95	1	0	0	Ee: ±1.3	Ee: ±0.5	Ee: ±0.8	Ee: ±2.1	
13	0	313	2	0	0	**4.0±0.8**	**0.0±0.0**	**94.4±0.8**	**1.5±0.5**	2
12	0	342	3	0	0	Et: ±0.6	Et: ±0.0	Et: ±0.8	Et: ±0.5	
18	0	348	3	0	0	Ee: ±0.8	Ee: ±0.0	Ee: ±0.8	Ee: ±0.2	

S5. Supporting Figures

Calibration of statistical measurements based on AFM

We have conducted a calibration measurement to verify one of our basic experimental assumption: the percentage of a species in AFM images accurately reflects its percentage in solution. We synthesized highly homogeneous flat and cyclized monomer solutions according to protocols described in the experimental section. Briefly, 4.2 nM scaffold was mixed with 10× staple and annealed to form flat monomer solution (*F1* solution). Separately, 4.2 nM scaffold was mixed with 10× staple and 200 nM linkers and annealed in one pot to form cyclized monomer solution (*C1* solution). The two solutions are of equal tile concentration, although the tile conformations are very different. Subsequently, the *F1* solution and the *C1* solution are mixed in different ratios to form standard calibration solutions. The calibration solutions were then imaged by AFM to measure the fraction of *C1*.

Figure S10 shows the measurement results for the calibration solutions. The raw AFM images are presented in Figure S11. As can be clearly seen, the measured *C1* fraction very accurately reflects the value expected from dilution. Considering the fact that the fraction of *C1* is close but not equal to 100 % in *C1* solution, the calibration curve is expected to have a slope slightly smaller than 1. Indeed, a linear fit of the calibration curve a slope of 0.98 ± 0.004, indicating that the fraction of *C1* is 98 ± 0.4 % in the one-pot annealed *C1* solution. Based on this highly linear calibration curve, we conclude that the fraction measurement by AFM in this study is unbiased between flat and cyclized species.

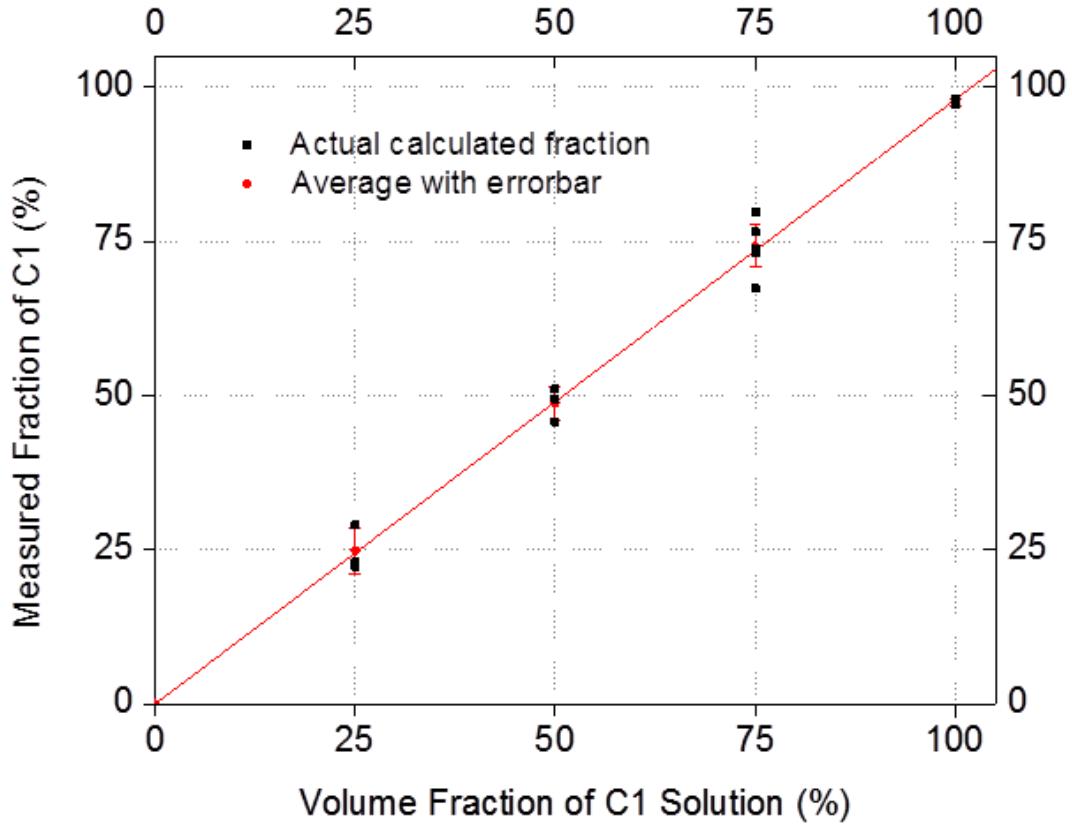

Figure S10: Calibration curve for the AFM fraction measurement method. The measured fraction of C1 (cyclized monomer) is plotted against the mixing ratio of the calibration solution. Black dot represents C1 percentage determined from one AFM image and the red dots represent average percentage obtained from all images taken for one sample.

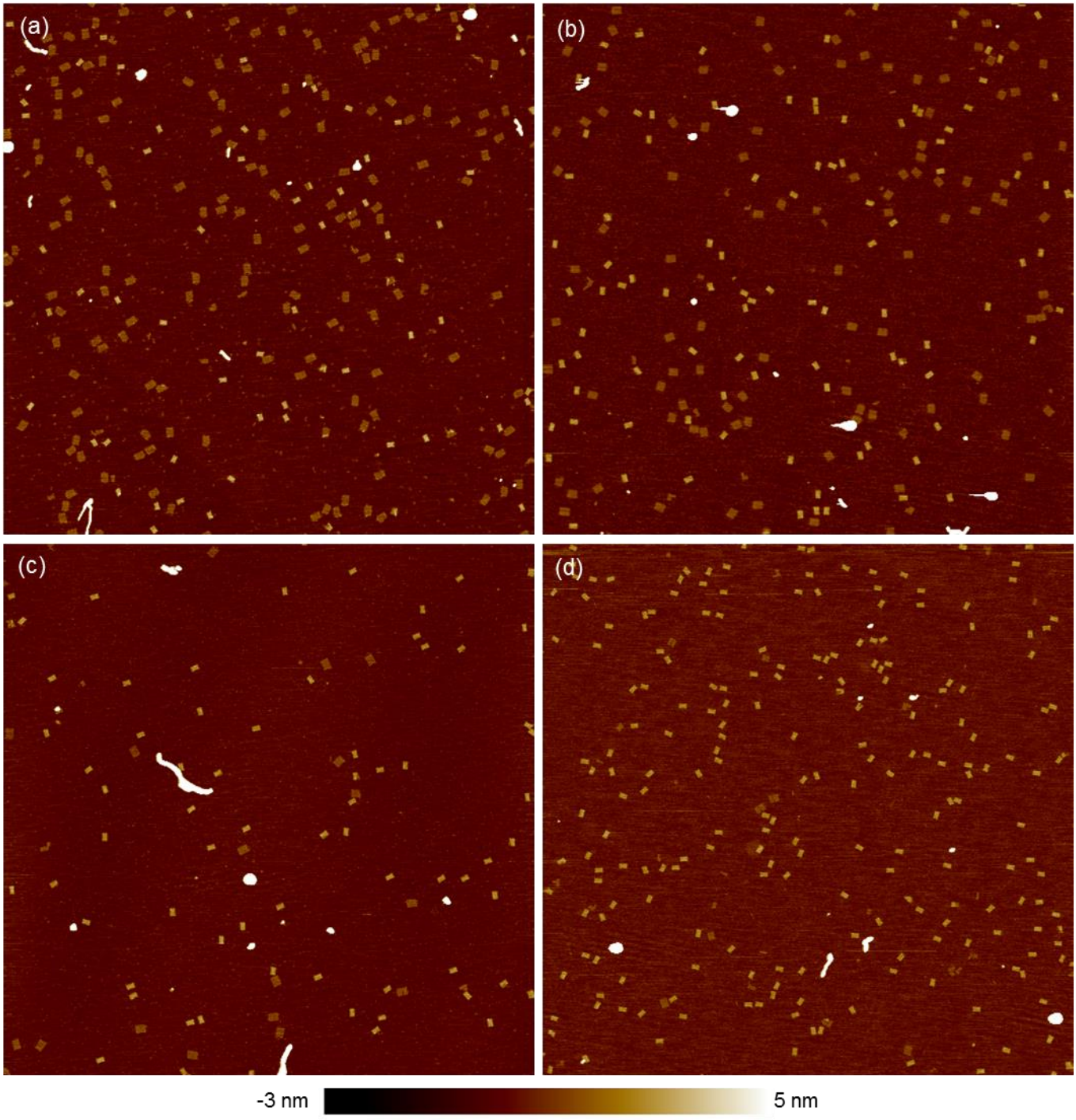

Figure S11: Original 5-µm × 5-µm AFM images taken for different standard calibration solutions: (a) mixture of 25% *C1* solution with 75% *F1* solution; (b) mixture of 50% *C1* solution with 50% *F1* solution; (c) mixture of 25% *C1* solution with 75% *F1* solution; (d) pure *C1* solution. From the images, *F1* and *C1* can be clearly distinguished by their size and contrast. *F1* tiles are dark yellow in color and larger in size, while *C1* tiles are bright yellow in color and smaller in size. The percentage of *C1* increases visibly to near 100% from (a) to (d).

Structural effect of missing staples

The structure of 32-helix tiles with 0, 7, 14 and 21 staples excluded are compared below in Figures S12 and S13. The tiles with 0, 7 and 14 staples missing retain their rectangular shape. The edges of the tiles are straight, even though some defects are present, partly due to the tearing by AFM tips. The tiles with 21 staples missing are distinctly different than the other three as many of them have curved and twisted edges. These curved tiles also tend to be elongated. Such phenomena can be found in both liquid-phase (Figure S12) and air-phase AFM (Figure S13). The images suggest that the tiles with 21 missing staples probably have compromised structural integrity.

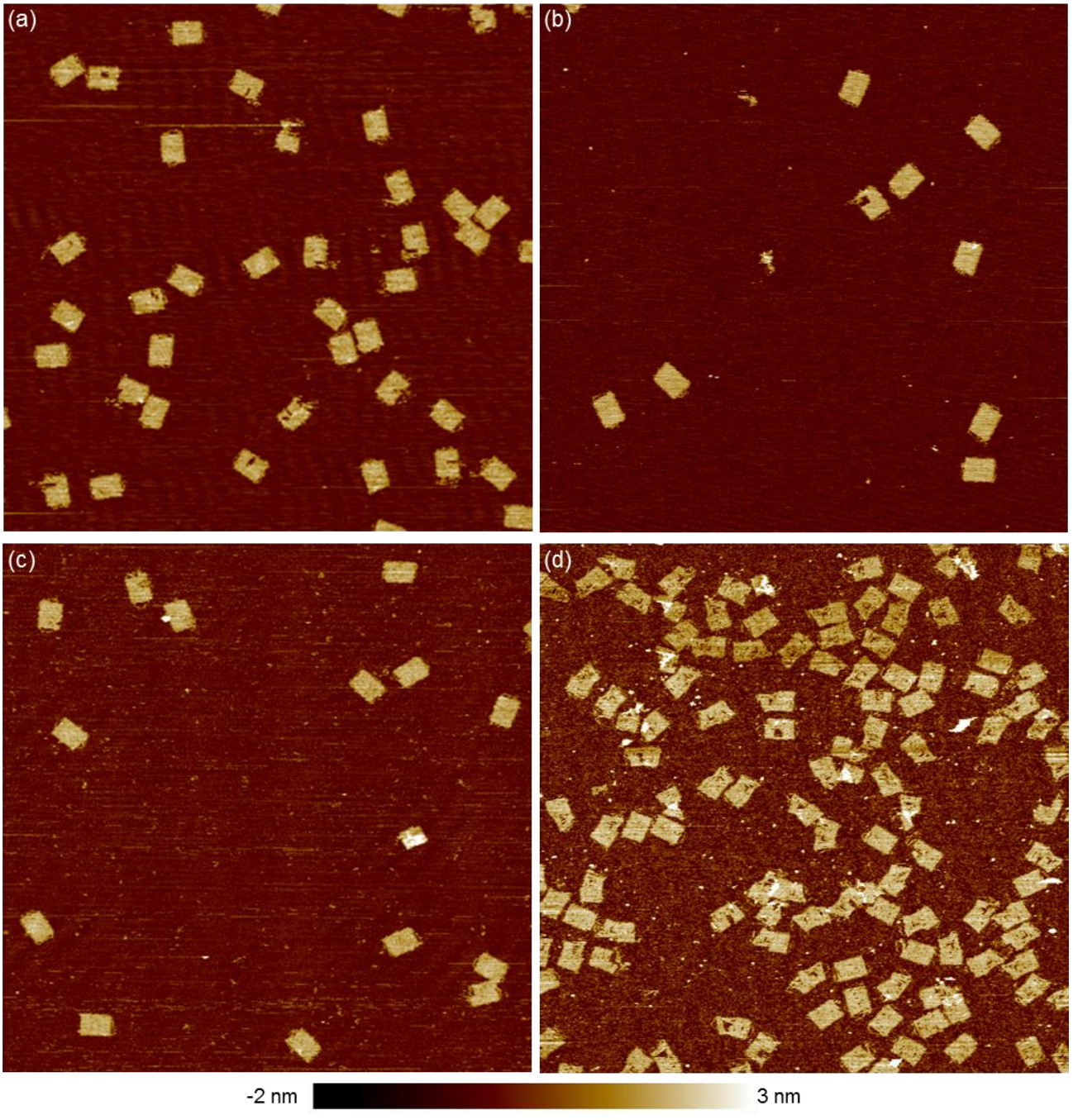

Figure S12: Liquid-phase AFM images of the 32-helix tiles with 0 staples (a), 7 staples (b), 14 staples (c) and 21 staples (d) excluded. Image size: 1.6 μm × 1.6 μm.

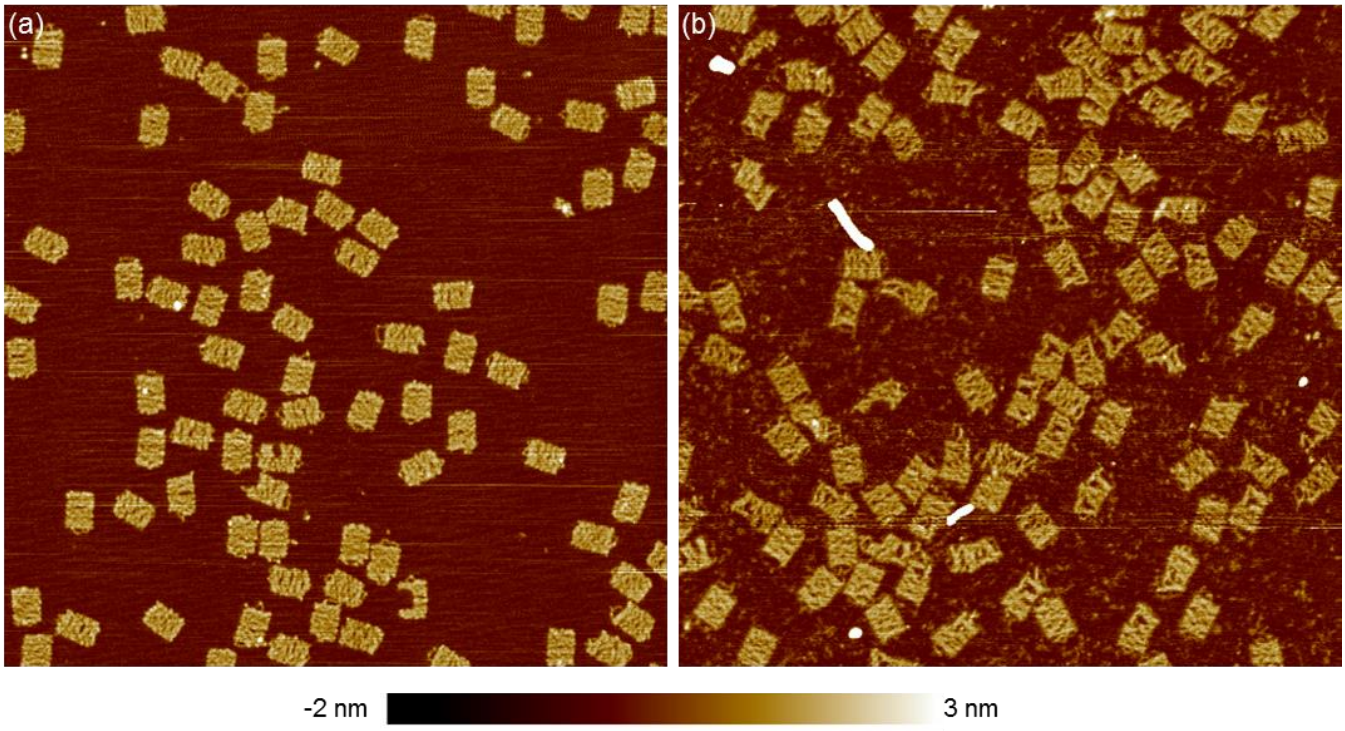

Figure S13: Air-phase AFM images of the 32-helix tiles with no staples missing (a) and 21 staples missing (b). The tiles with 21 staples missing frequently have curved or twisted edges. These tiles also tend to have a big hole in the middle and be more elongated. Image size: 1.6 μm × 1.6 μm.

Determination of origami monomer concentration and melting temperature

Fluorescence correlation spectroscopy (FCS) was performed with the Microtime200 scanning confocal time-resolved microscope (Picoquant GmbH). A 467 nm picosecond pulsed laser was delivered to the sample stage through an apochromatic 60×, 1.2 N.A. water immersion objective to excite the FAM on DNA origami. The emitted fluorescence signal was collected with the same objective, in addition with a dual band dichroic (z467/638rpc, Chroma) to filter out the scattered excitation light. A 50-μm pinhole was further employed to block the off-focus photons, and the final signal was additionally filtered by a narrow-band filter (520 ± 20 nm, Chroma) before reaching the single photon avalanche photodiode detector (SPAD, SPCM-AQR, PerkinElmer Inc.). Fluorescence signals were recorded using the time-tagged time-resolved (TTTR) mode (TimeHarp200), and the generated autocorrelation function was analyzed by the SymPhoTime software package (PicoQuant GmbH). In definition, autocorrelation function describes the similarity between observations as a function of lag time (τ):

$$G(\tau) = \frac{\langle \delta F(t) \cdot \delta F(t+\tau) \rangle}{\langle F(t) \rangle^2} .$$

For the fluorescent molecules diffusing in a 3D confocal volume, it can be expressed as:

$$G(\tau) = \frac{1}{\langle N \rangle}\left(1+\frac{\tau}{\tau_D}\right)^{-1}\left(1+\frac{\tau}{\kappa^2\tau_D}\right)^{-1/2},$$

where <N> is the average number of diffusors in the detection volume and $G(0) = 1/\langle N \rangle$. κ is the ratio of lateral (w_0) to axial (z_0) radii of excitation beam, and τ_D is the molecular diffusion time[12]. The effective volume can be calculated by: $V_{eff} = \pi^{3/2} w_0^2 z_0$, which was calibrated to be 0.9 fL for our system. Hence, the molecular concentration can be determined as:

$$\langle C \rangle = \frac{1}{G(0) \cdot V_{eff}} .$$

Melting curves of the origami tiles were measured to determine the highest viable incubation temperature. Fluorescence signals from flat and folded origami monomers were simultaneously monitored in a RT-PCR machine while the temperature was increased at a rate of 2 °C/min. For folded origami, a clear transition of the fluorescence curve is visible between 55 to 65 °C, corresponding to the spontaneous opening of the folded tiles. To ensure the structural integrity of the folded origami species, incubation temperatures were kept at or below 50 °C.

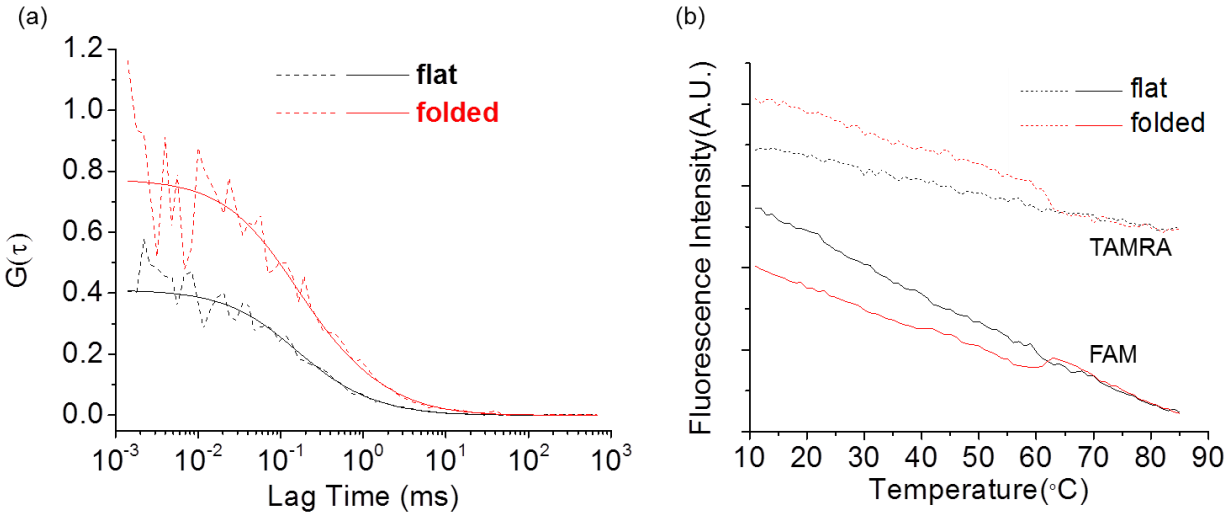

Figure S14: (a) Fluorescence correlation spectra of the flat and folded origami monomers. Experimental data points for flat and folded origami are shown as black and red dash lines, respectively. Fitted curves are also presented as solid lines of corresponding colors. (b) Melting curves of the flat (black) and folded (red) origami monomers. Distinct transition occurs between 55 and 65 °C.

Vertical linking vs horizontal linking

The origami rectangle has two pairs of opposite edges. Correspondingly, there are two ways of connecting the edges, as illustrated in Figure S15. Connecting vertically leads to poor oligomerization, whereas connecting horizontally easily results in long origami chains. AFM results for our 32–helix tile oligomerization is also presented here. Both samples were incubated at 40 °C for 2 hours with respective 200 nM linker strands. The number of linkers for horizontal linking was reduced to 13 to match the number for vertical linking. While vertical linking never produces chains longer containing 4-tiles, horizontal linking achieves over 1-μm-long chains (over 14-tiles). The near periodical twisting of the long horizontally connected chain also clearly suggests the global twisting of the monomer tile.

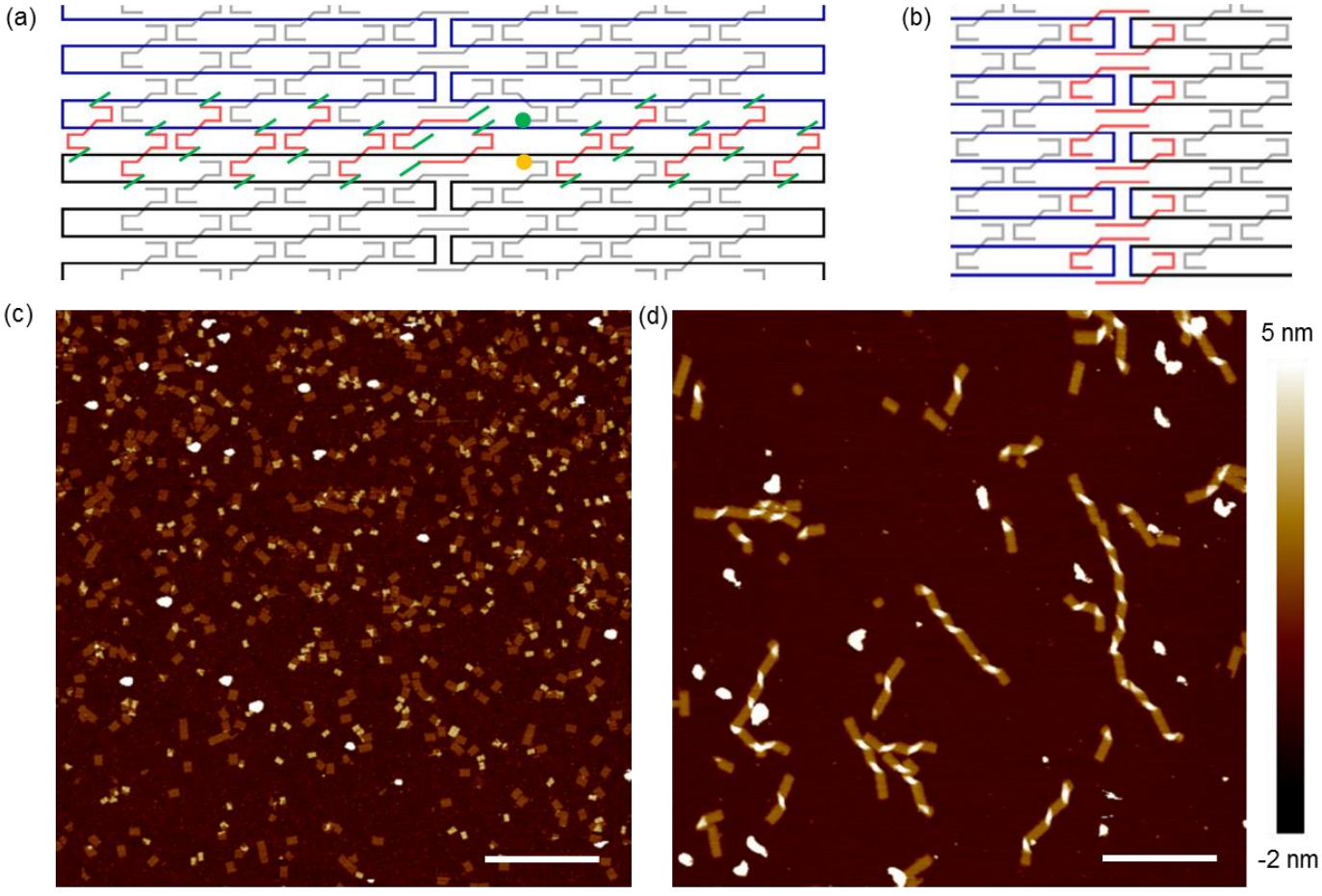

Figure S15: (a)-(b) Strand folding path details for the two schemes of linking origami: (a) vertical linking and (b) horizontal linking. Linkers are shown in red. Scaffold strands of different origami tiles are shown in black and blue. Normal staples are presented in gray. (c)-(d) Corresponding AFM images of the linking results: (c) vertical linking and (d) horizontal linking. Scale bar: 1 μm.

The effect of linker number on folding yield

Folding yield was examined as a function of number of linkers by incubating the 32-helix tile with 7 missing staples at 40 °C for 1 hour. The concentration for linkers was kept at 200 nM, while the number of linkers was varied. A sharp increase of folding yield (percentage of *C1*) was observed when the number of linkers was increased from 5 to 6. The minimum number of linkers for folding is therefore concluded to be 6.

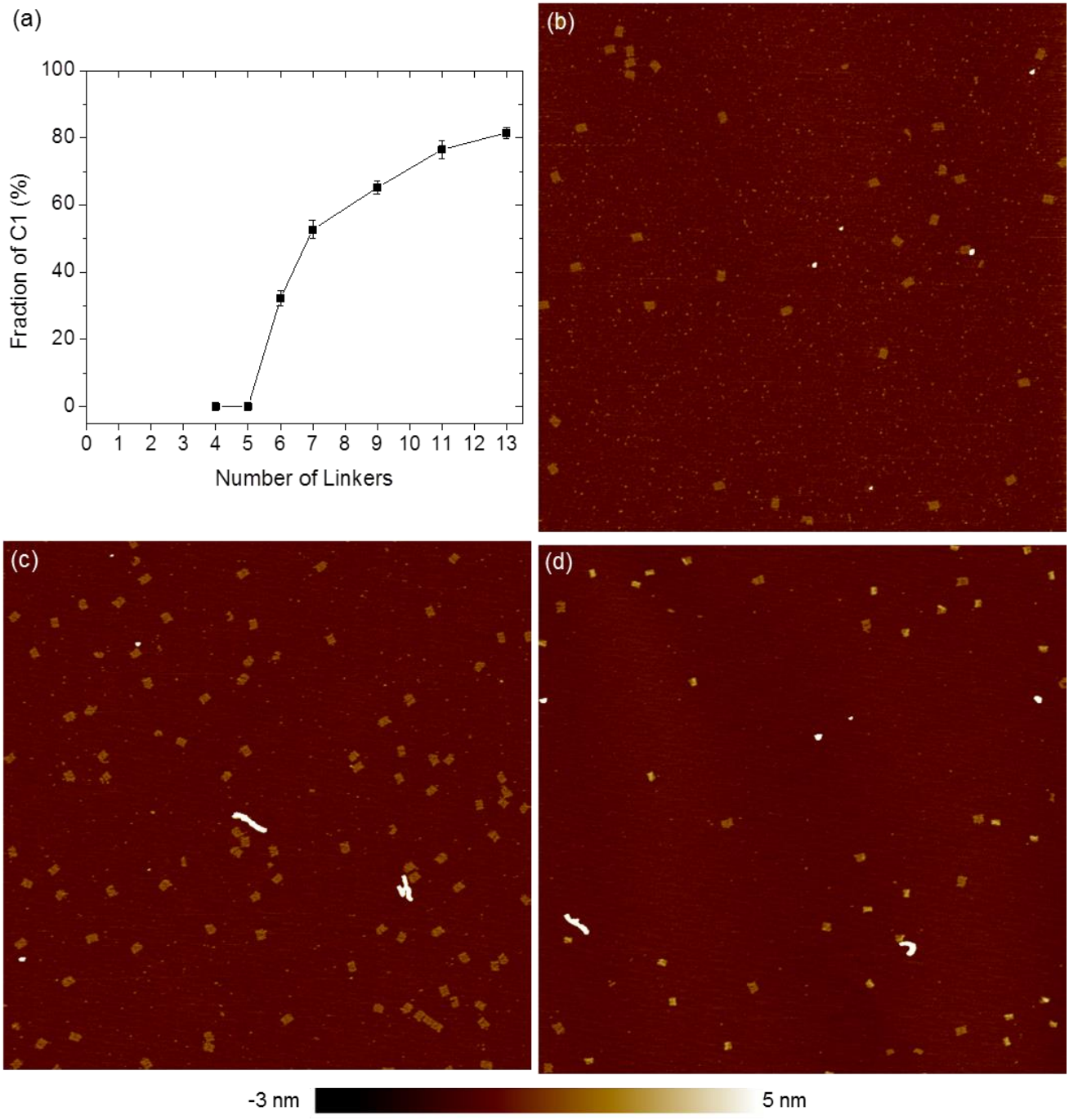

Figure S16: (a) Percentage of *C1* species as a function of linker number after folding. (b)-(c) Raw AFM images after folding origami tiles at 40 °C for 1 hour with 4 linkers (b), 5 linkers (c) and 6 linkers (d). *C1* species begin to appear for 6 linkers (d). Image size: 5 µm × 5 µm.

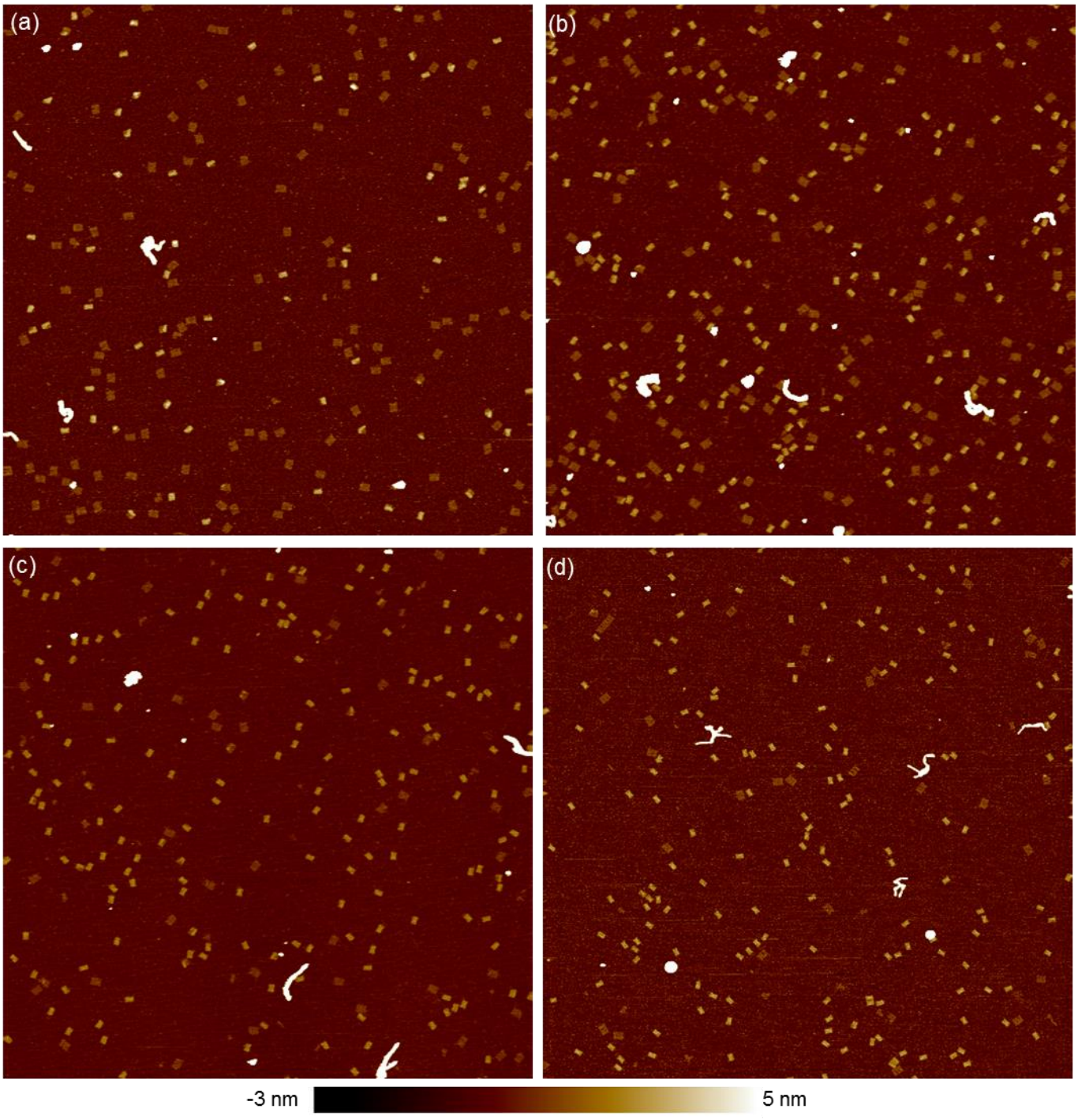

Figure S17: Raw AFM images after folding origami tiles at 40 °C for 1 hour with 7 linkers (a), 9 linkers (b), 11 linkers (c), and 13 linkers (d). The percentage of *C1* species increases steadily as linker number increases. Image size: 5 μm × 5 μm.

Estimation of the energy gain of one linker

The average energy gain from the hybridization of an 8-base-long strand of random sequence can be calculated from the nearest neighbor model[13]. For a 8-base-long strand, there are 7 nearest neighbor pairs. Therefore, $\overline{\Delta G} = 7 \cdot \overline{\Delta G_{nn}} + \overline{\Delta G_{initial}}$ = -8.8 kcal/mol. The calculation of $\overline{\Delta G_{nn}}$ and $\overline{\Delta G_{initial}}$ at T = 40 °C = 313.15 K, 1 M Na^+ is presented in the following table.

Table S2: Calculation of the average binding energy of a nearest neighbor pair and the average initial binding energy. Numbers with gray background are from reference[13].

Permutation of nearest neighbors	ΔH (kcal/mol)	ΔS (cal/mol·K)	ΔG = ΔH-T·ΔS (kcal/mol)
AA/TT	-7.9	-22.2	-0.94807
AT/AT	-7.2	-20.4	-0.81174
AC/GT	-8.4	-22.4	-1.38544
AG/CT	-7.8	-21	-1.22385
TA/TA	-7.2	-21.3	-0.529905
TT/GG	-8	-19.9	-1.768315
TC/GA	-8.2	-22.2	-1.24807
TG/CA	-8.5	-22.7	-1.391495
CA/TG	-8.5	-22.7	-1.391495
CT/AG	-7.8	-21	-1.22385
CC/GG	-8	-19.9	-1.768315
CG/CG	-10.6	-27.2	-2.08232
GA/TC	-8.2	-22.2	-1.24807
GT/AC	-8.4	-22.4	-1.38544
GC/GC	-9.8	-24.4	-2.15914
GG/CC	-8	-19.9	-1.768315
Average ΔG_{nn}			-1.395864375
Initial ΔG with terminal G·C	0.1	-2.8	1.00482
Initial ΔG with terminal A·T	2.3	4.1	0.975085
Average $\Delta G_{initial}$			0.9899525
			-8.781098125

Equilibrium conformation as a function of missing staples:

Simulation results from CanDo suggests that the global equilibrium conformation is not significantly affected by the isolated single-strand holes created by eliminating staples.

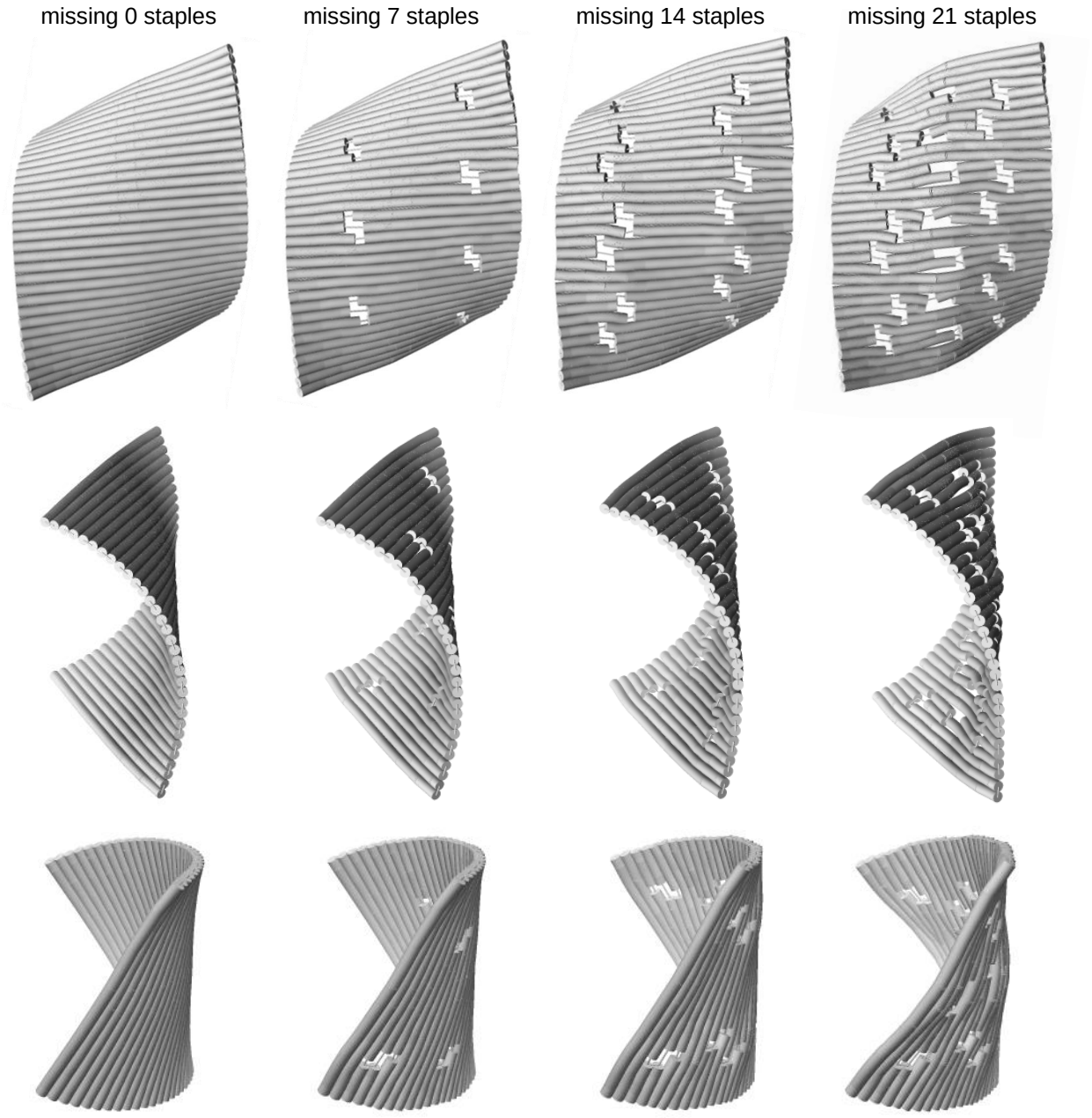

Figure S18: CanDo simulation results of equilibrium structure for origami rectangles with various numbers of missing staples. The global conformation is not visibly changed.

Origami tiles of shorter height

Origami tiles of shorter height can be synthesized by eliminating consecutive rows of staples from the original design. As illustrated below, 10 or 5 consecutive rows of staples were eliminated to produce 12-helix and 22-helix tiles of the same width as our original 32-helix tile.

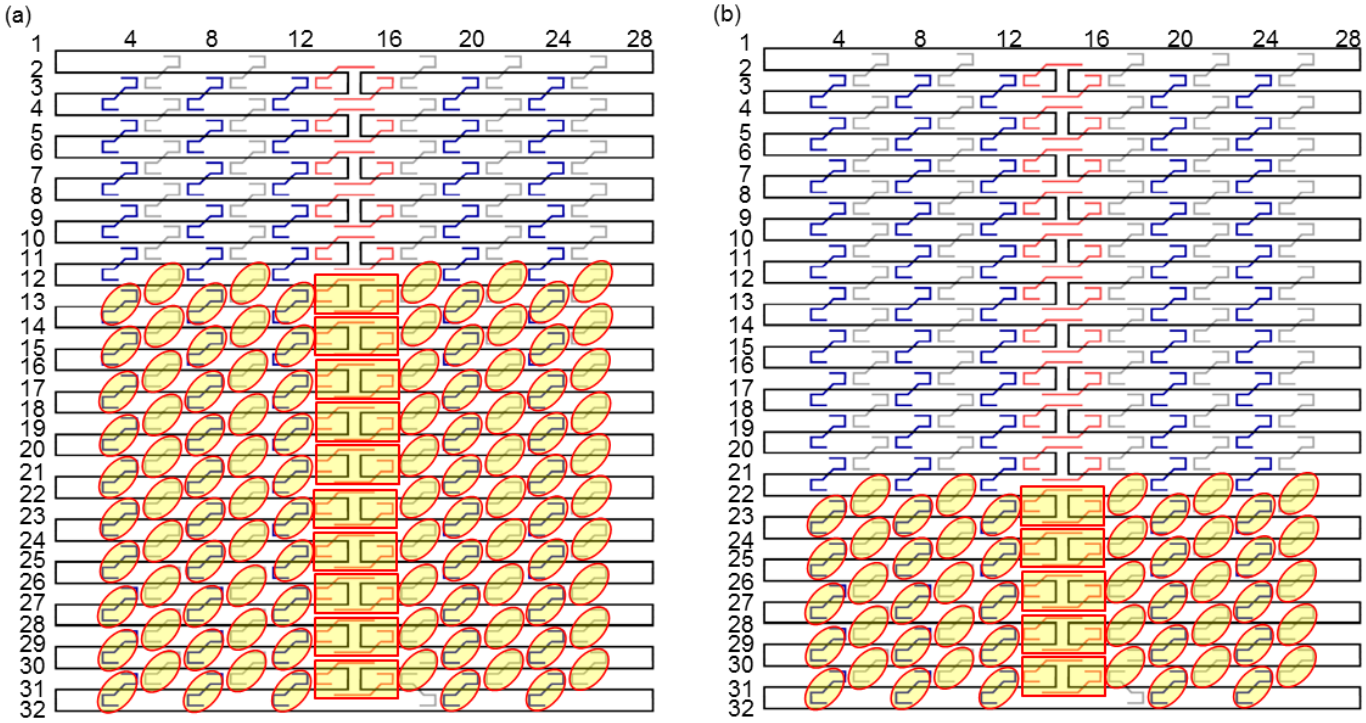

Figure S19: (a)-(b) Folding path diagram of 12-helix (a) and 22-helix origami tiles (b). The omitted staples are highlighted.

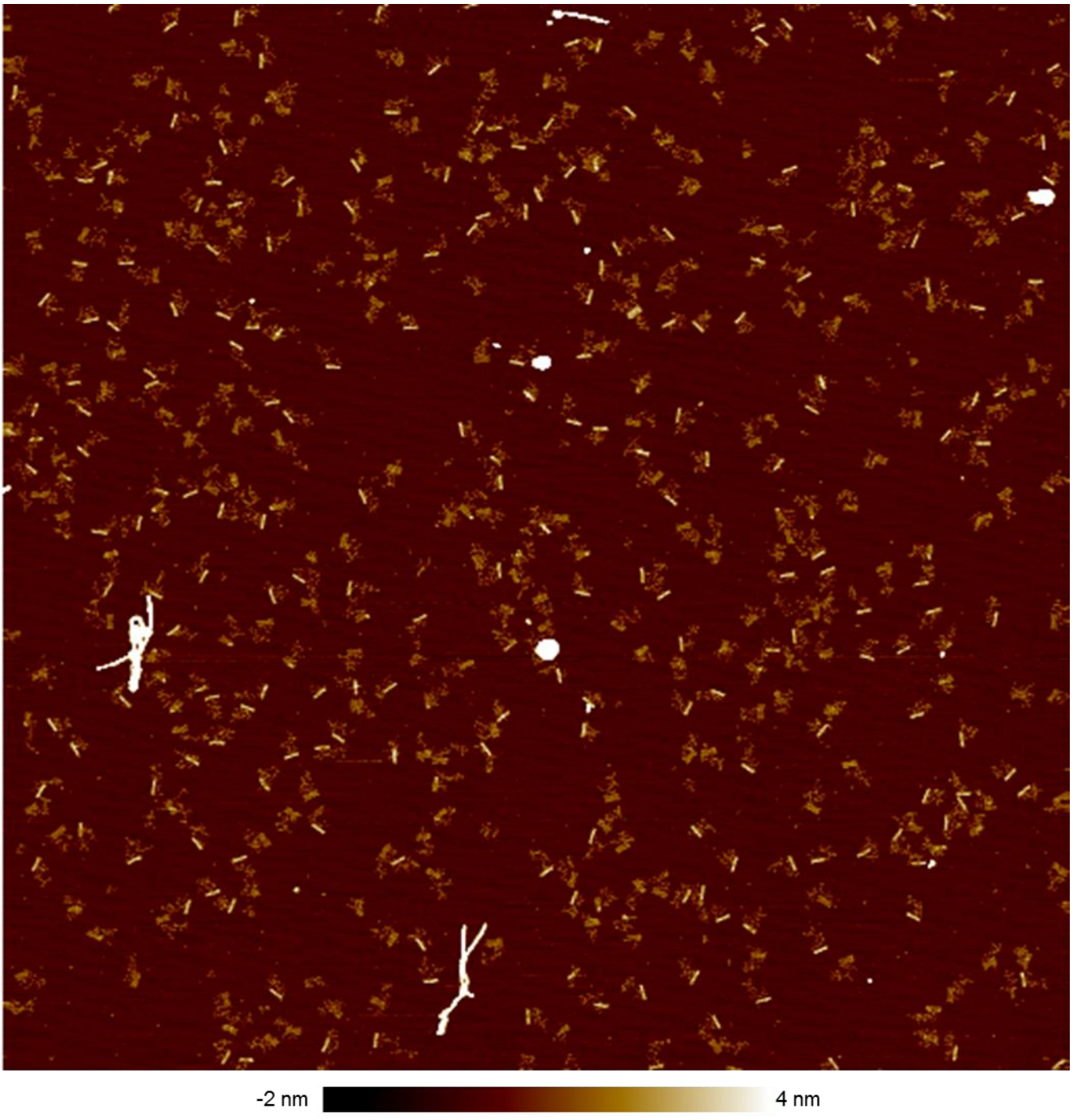

Figure S20: 5-μm × 5_μm AFM image for counting the percentage of folded 12-helix tiles after incubating at 40 °C for 0.5 hour.

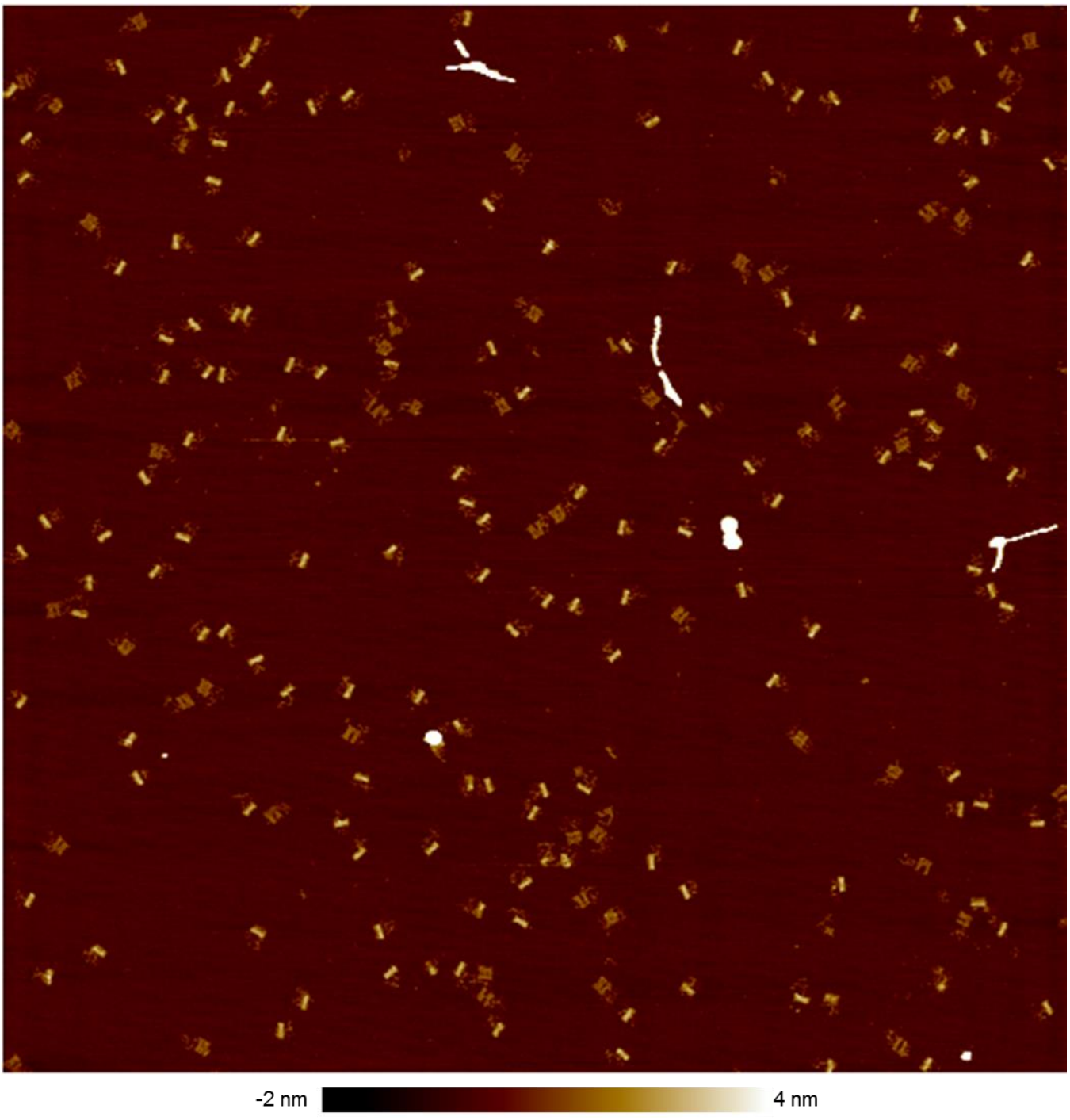

Figure S21: 5-μm × 5-μm AFM image for counting the percentage of folded 22-helix tiles after incubating at 40 °C for 0.5 hour.

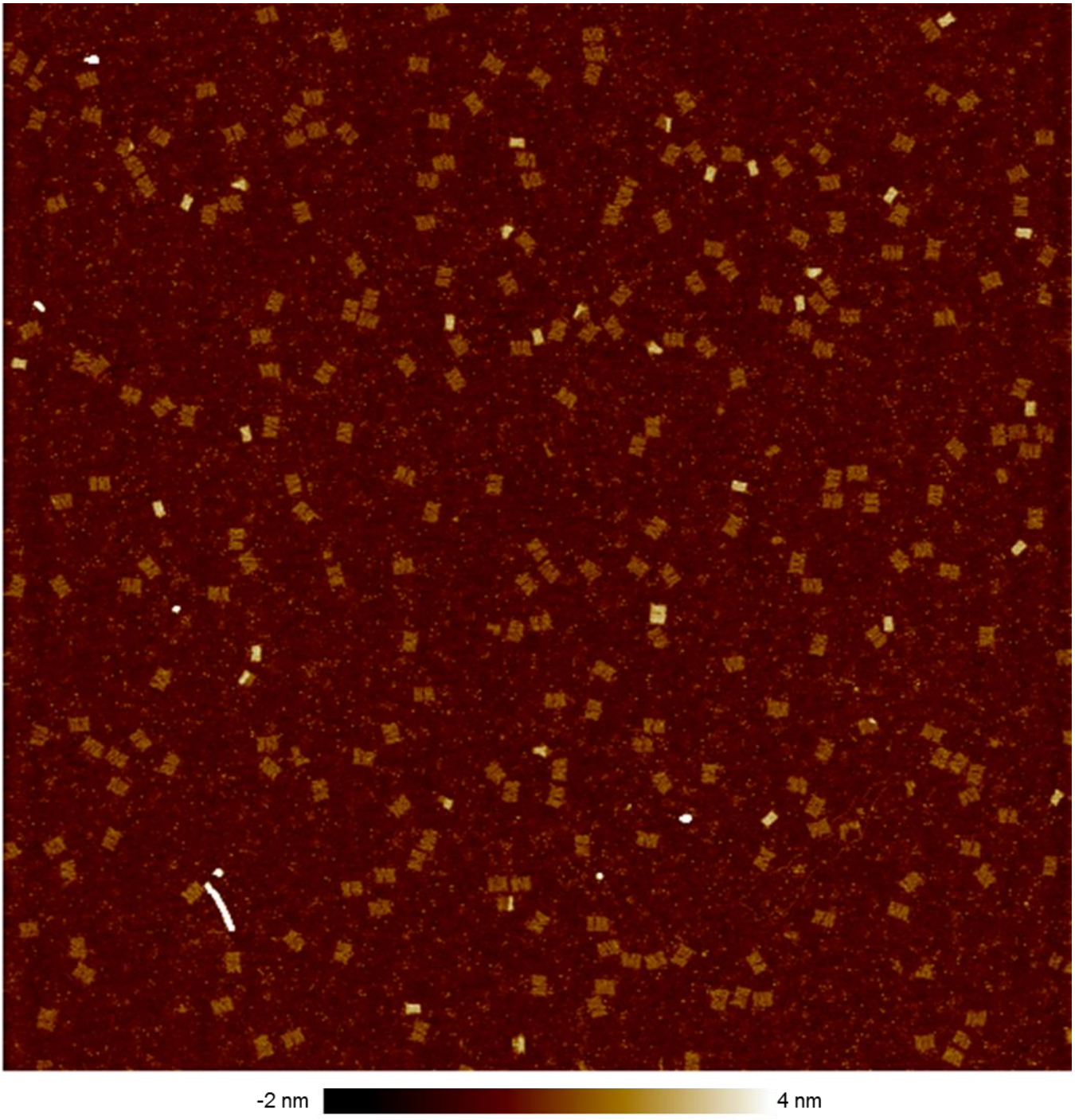

Figure S22: 5-μm × 5-μm AFM image for counting the percentage of folded 32-helix tiles after incubating at 40 °C for 0.5 hour.

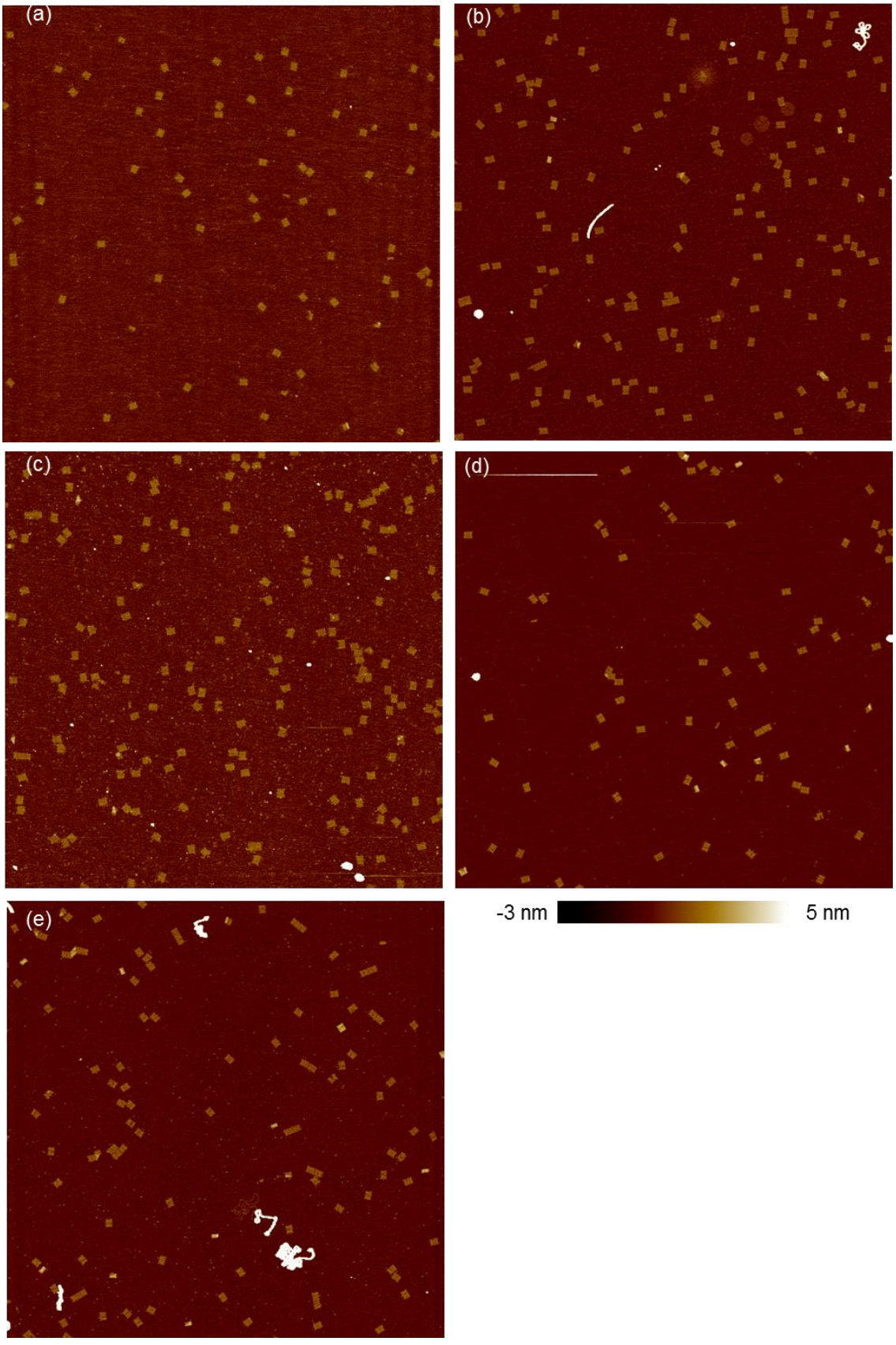

Figure S23: 5-µm × 5-µm AFM images after folding reaction at 35 °C from 4.2 nM. Incubation time: 0.5 hour (a), 1 hour (b), 2 hours (c), 4 hours (d), and 8 hours (e).

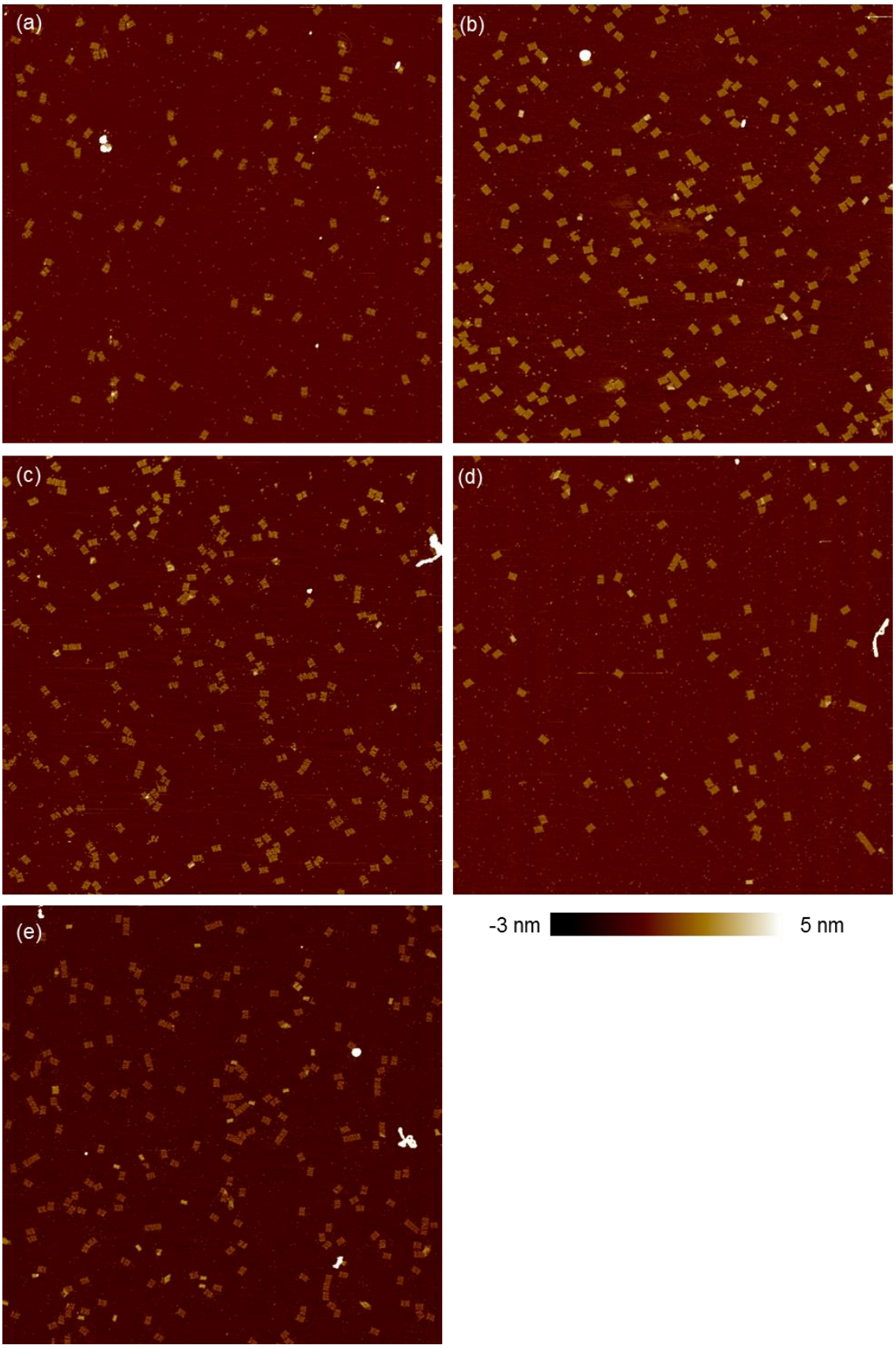

Figure S24: 5-µm × 5-µm AFM images after folding reaction at 35 °C from 1.3 nM. Incubation time: 0.5 hour (a), 1 hour (b), 2 hours (c), 4 hours (d), and 8 hours (e).

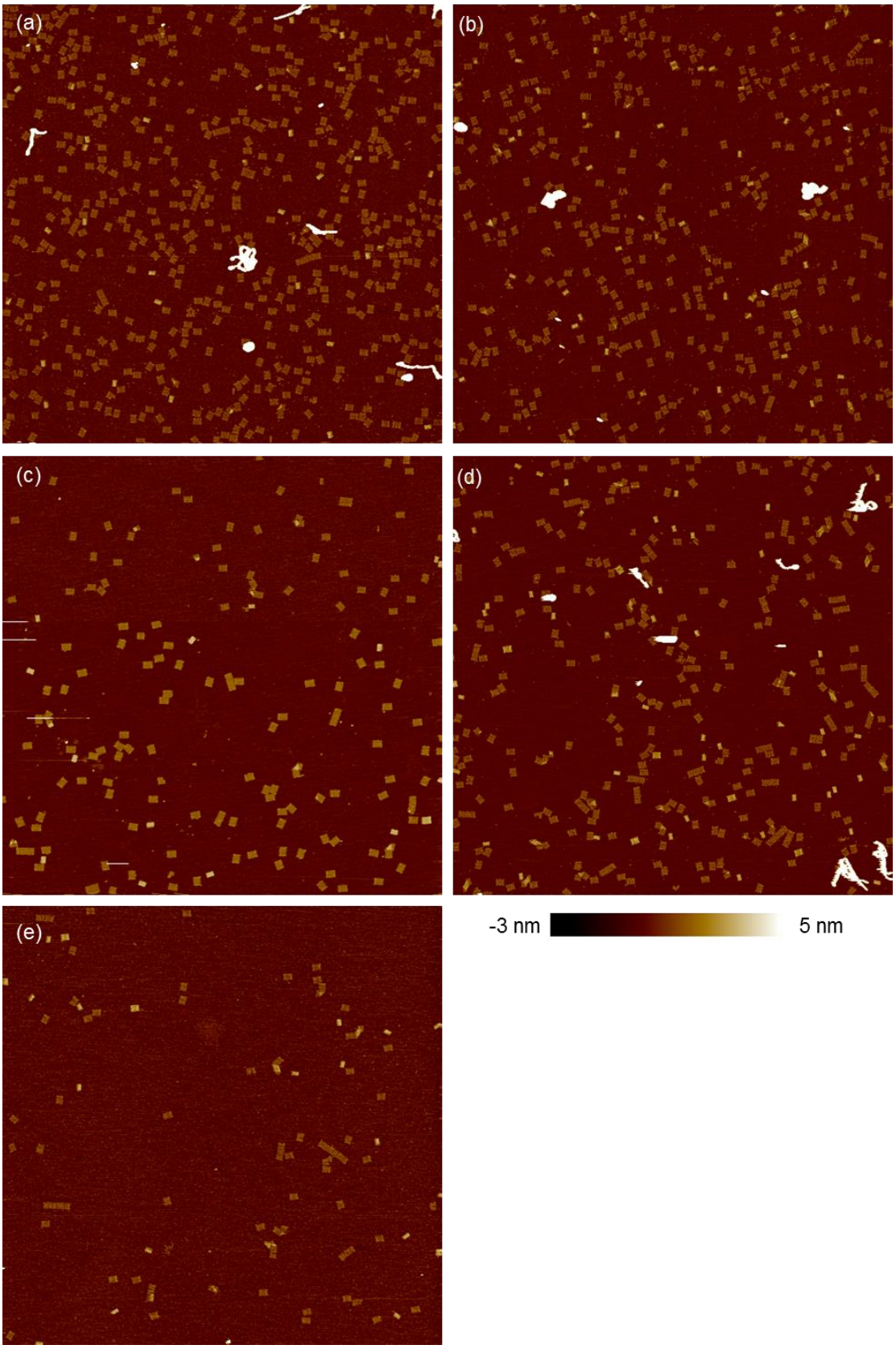

Figure S25: 5-µm × 5 µm AFM images after folding reaction at 40 °C from 4.2 nM. Incubation time: 0.5 hour (a), 1 hour (b), 2 hours (c), 4 hours (d), and 8 hours (e).

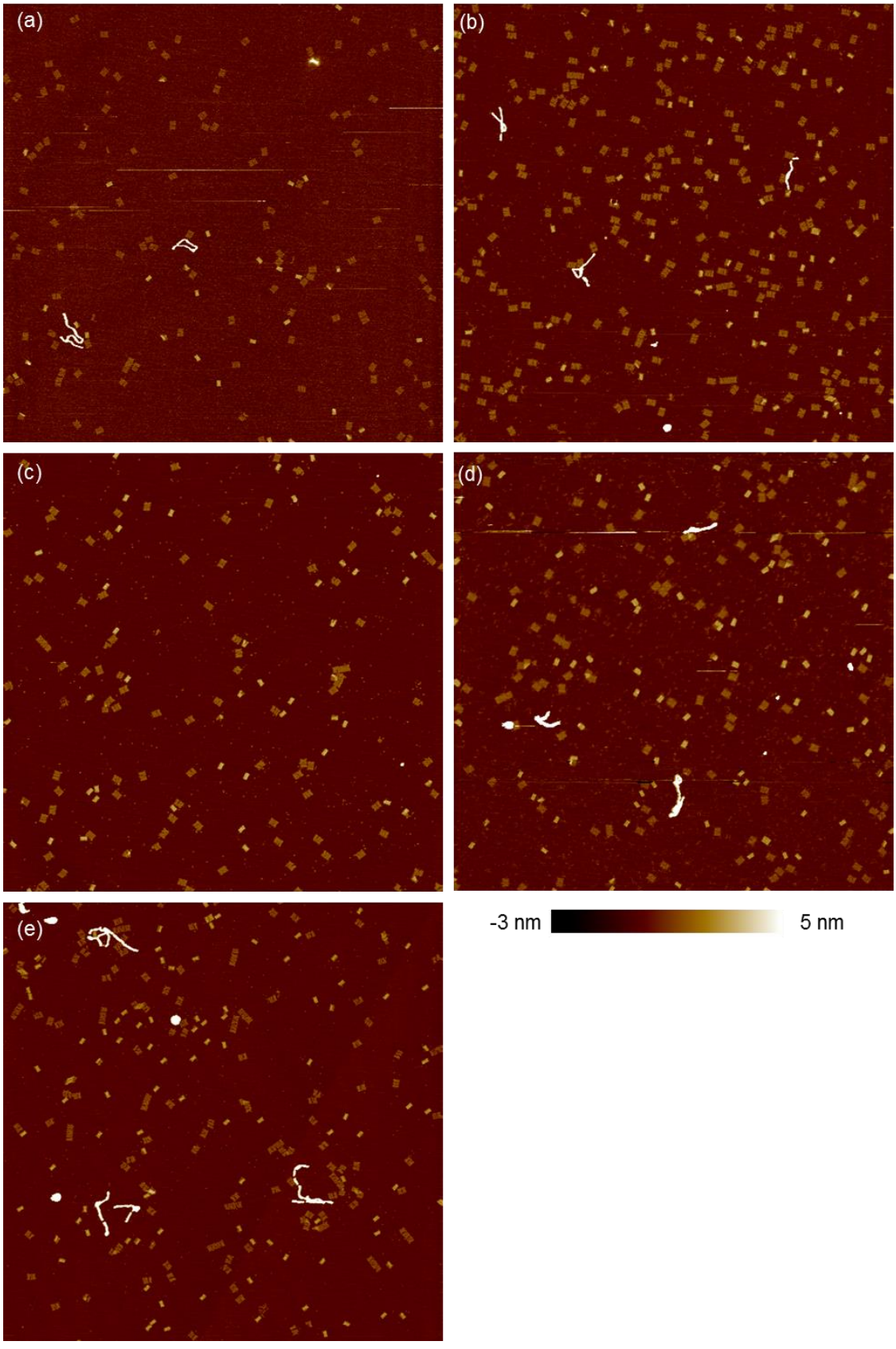

Figure S26: 5-µm × 5-µm AFM after folding reaction at 40 °C from 1.3 nM. Incubation time: 0.5 hour (a), 1 hour (b), 2 hours (c), 4 hours (d), and 8 hours (e).

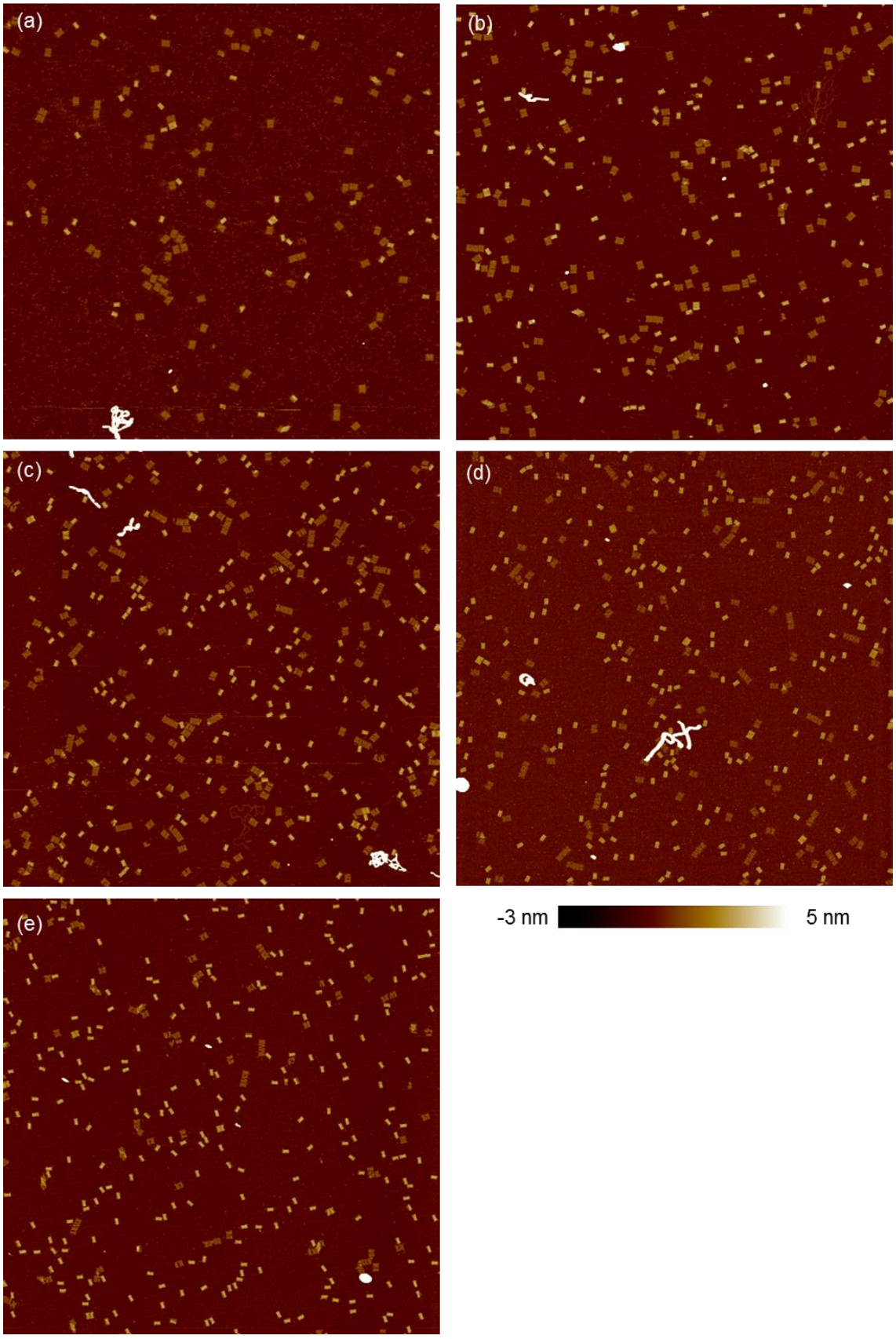

Figure S27: 5-µm × 5-µm AFM images after folding reaction at 45 °C from 4.2 nM. Incubation time: 0.5 hour (a), 1 hour (b), 2 hours (c), 4 hours (d), and 8 hours (e).

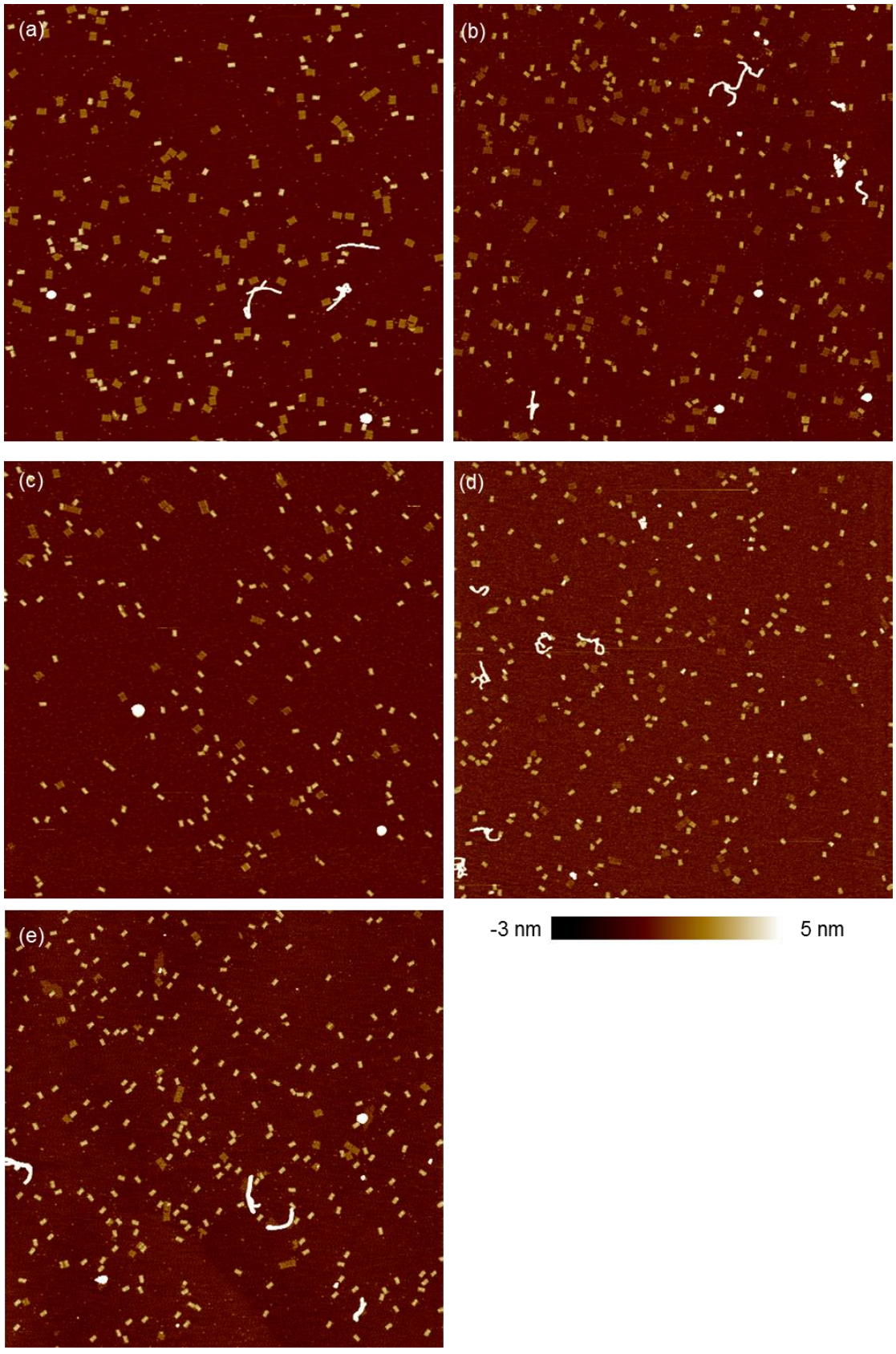

Figure S28: 5-µm × 5-µm AFM images after folding reaction at 45 °C from 1.3 nM. Incubation time: 0.5 hour (a), 1 hour (b), 2 hours (c), 4 hours (d), and 8 hours (e).

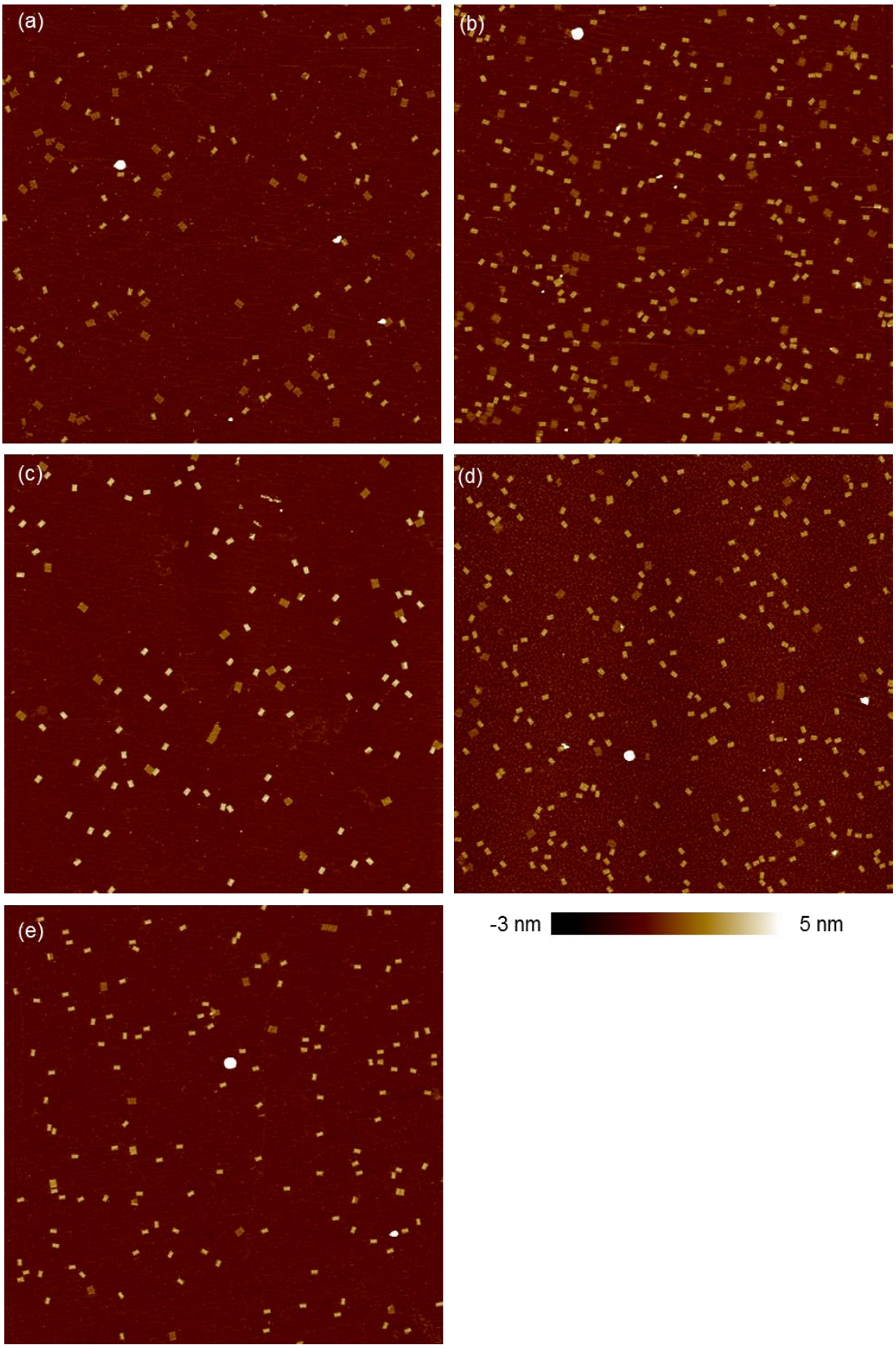

Figure S29: 5-µm × 5-µm AFM images after folding reaction at 50 °C from 4.2 nM. Incubation time: 10 minutes (a), 20 minutes (b), 30 minutes (c), 1 hour (d), and 2 hours (e).

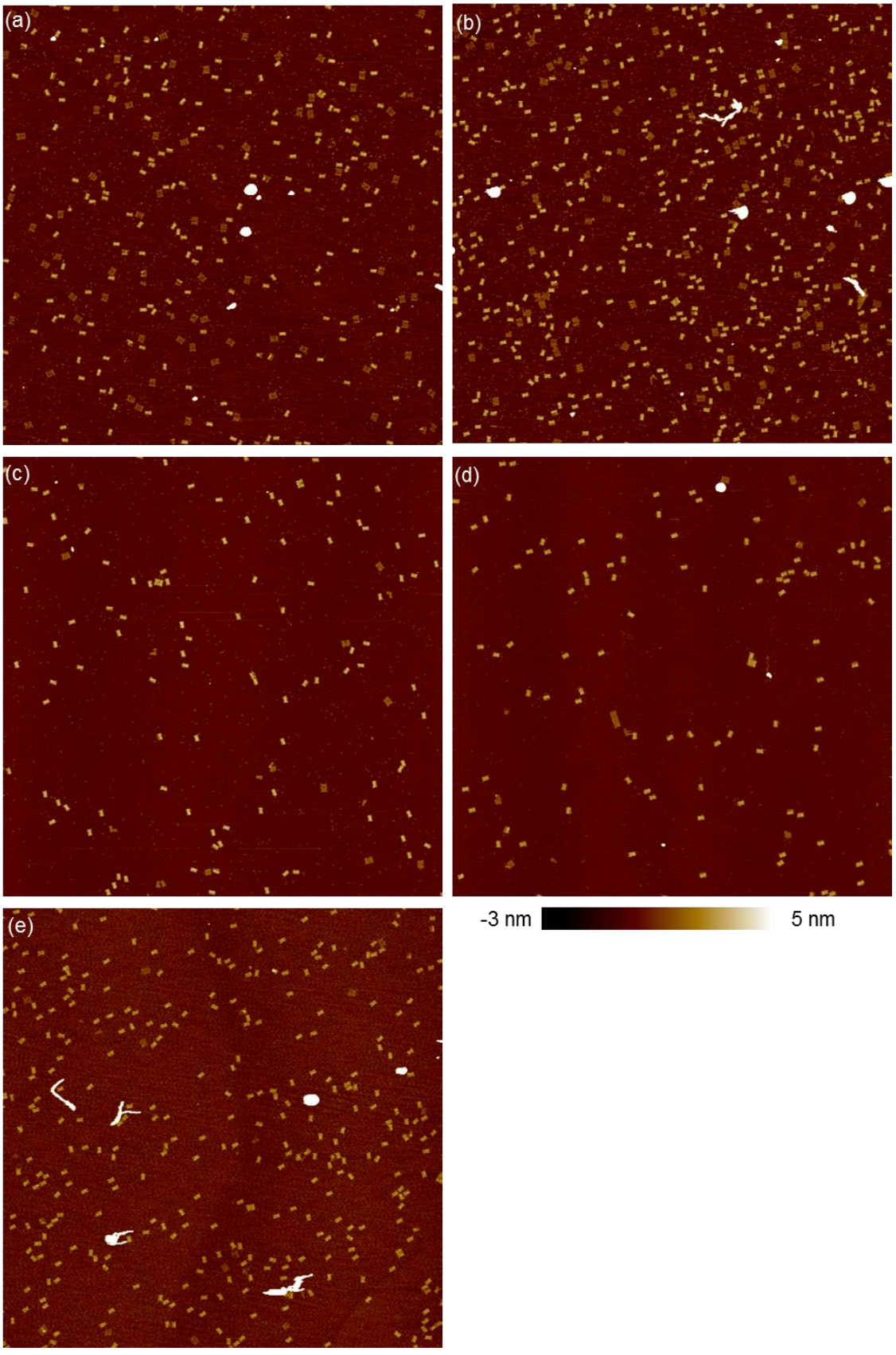

Figure S30: 5-µm × 5-µm AFM images after folding reaction at 50 °C from 1.3 nM. Incubation time: 10 minutes (a), 20 minutes (b), 30 minutes (c), 1 hour (d), and 2 hours (e).

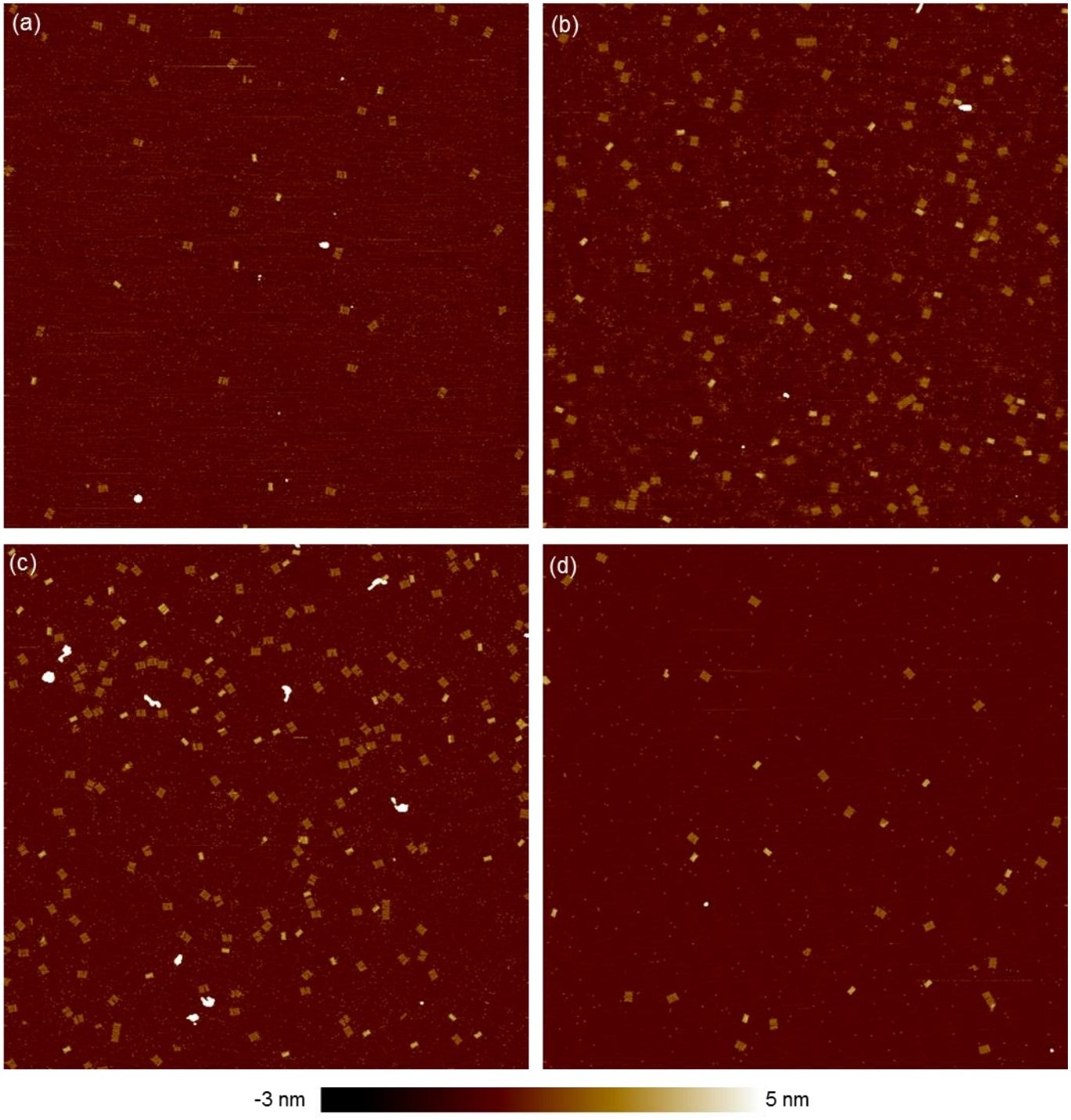

Figure S31: 5-μm × 5-μm AFM images for folding process of the tiles with no missing staples (at 40 °C). Incubation time: 0.5 hour (a), 1 hour (b), 2 hours (c), and 4 hours (d).

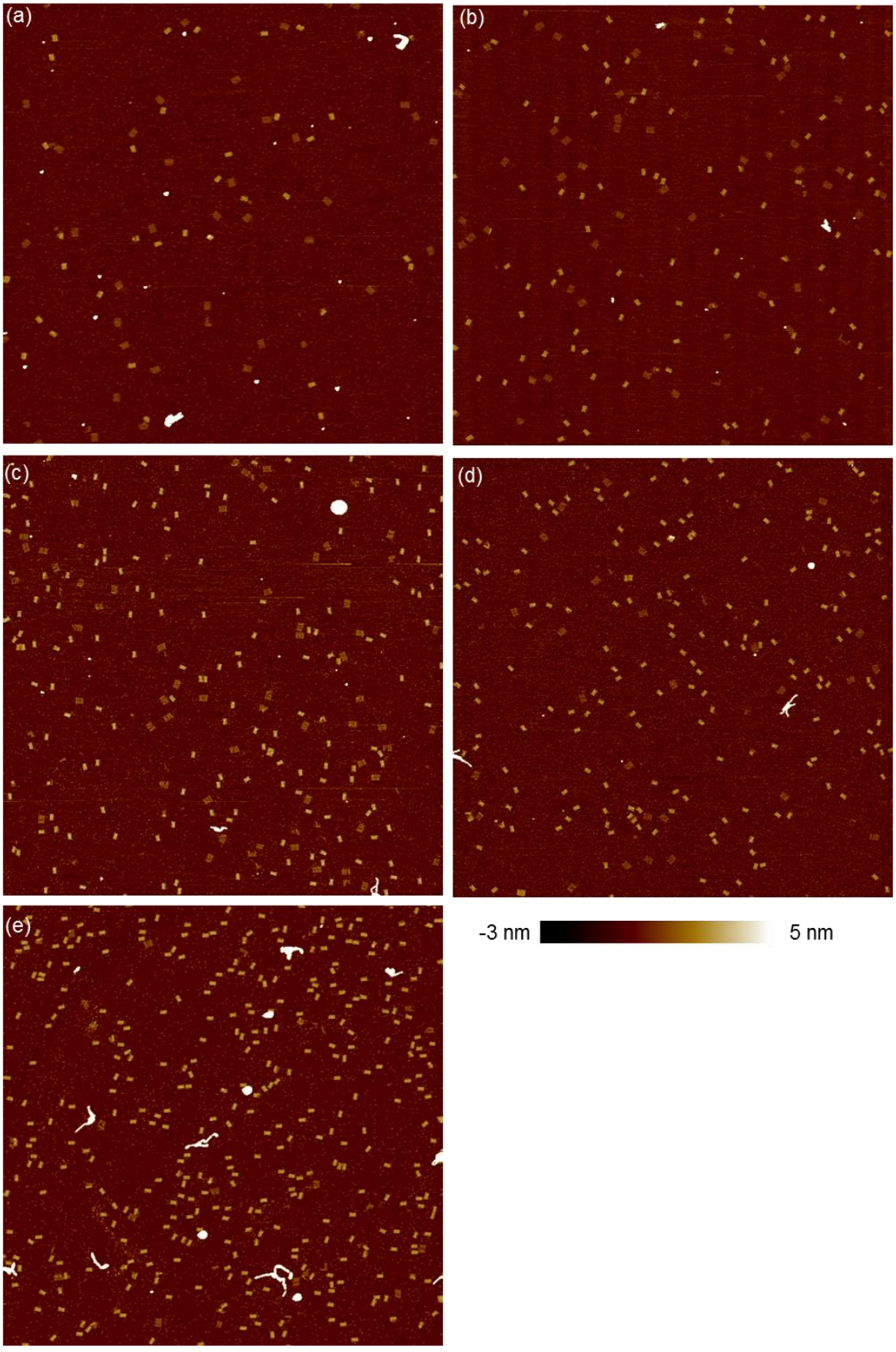

Figure S32: 5-µm × 5-µm AFM images for folding process of the tiles with 7 missing staples (at 40 °C). Incubation time: 10 minutes (a), 20 minutes (b), 30 minutes (c), 1 hour (d), and 4 hours (e).

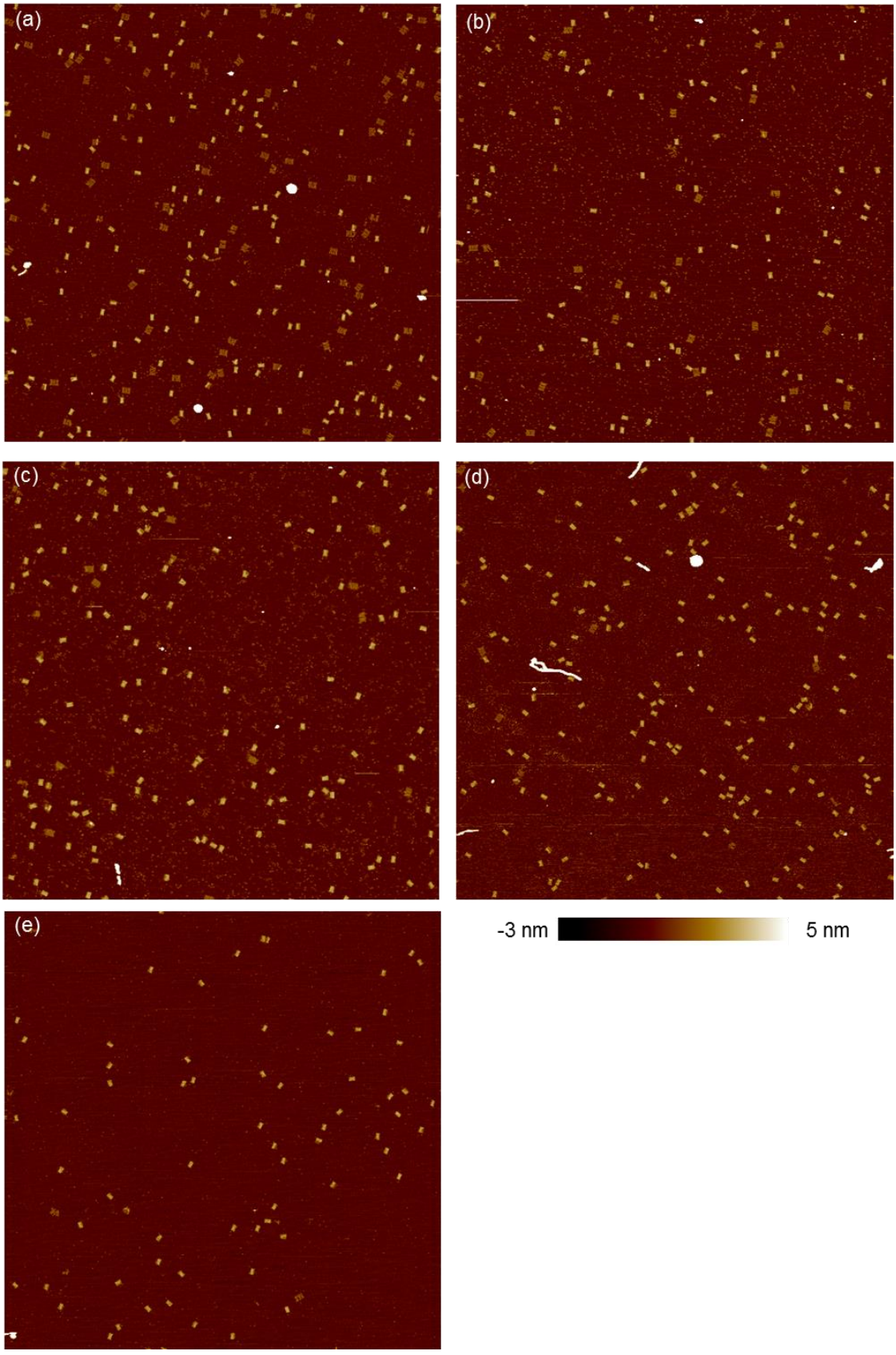

Figure S33: 5-µm × 5-µm AFM images for folding process of the tiles with 14 missing staples (at 40 °C). Incubation time: 10 minutes (a), 20 minutes (b), 30 minutes (c), 1 hour (d), and 4 hours (e).

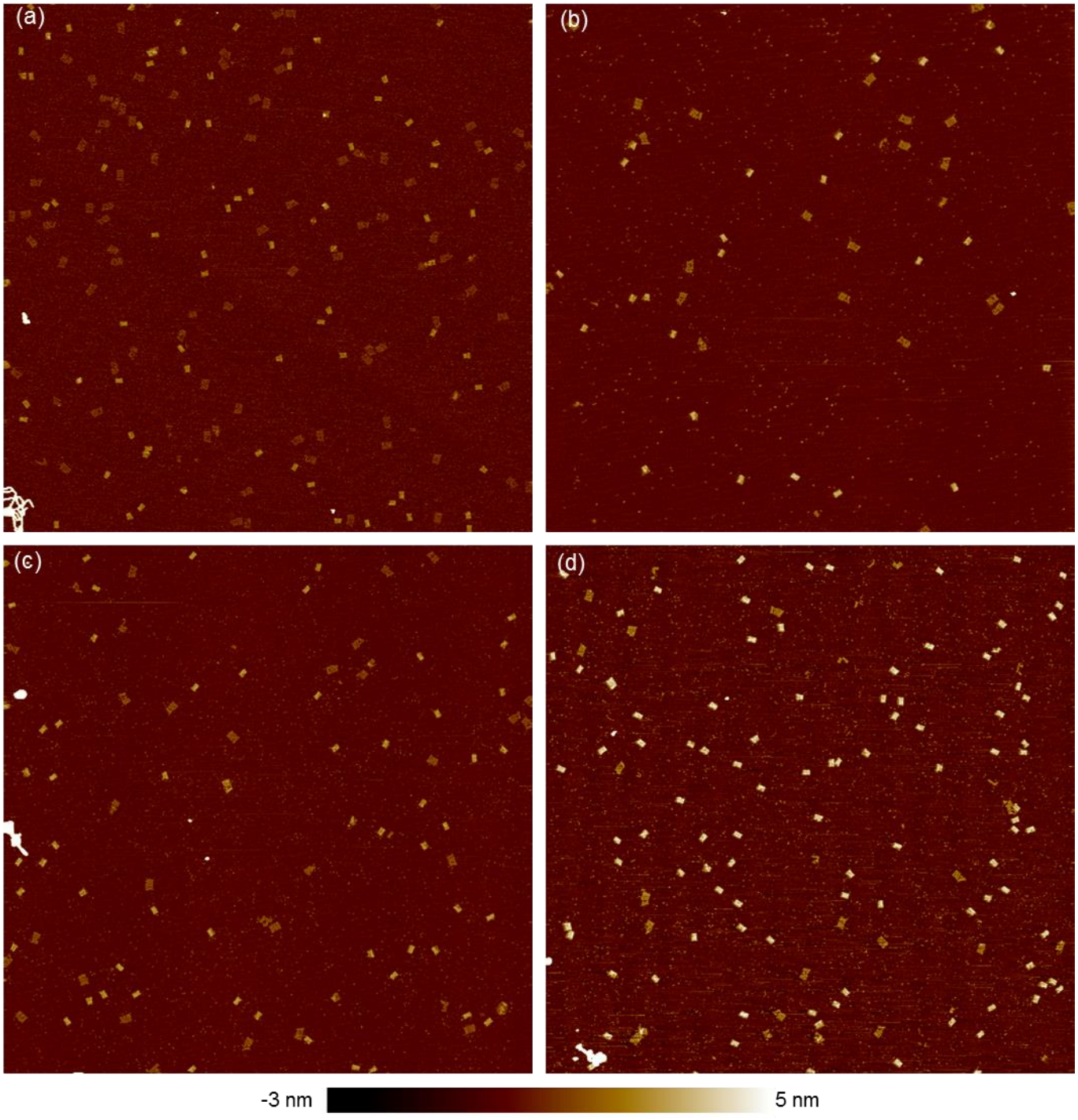

Figure S34: 5-µm × 5-µm AFM images for folding process of the tiles with 21 missing staples (at 40 °C). Incubation time: 0.5 hour (a), 1 hour (b), 2 hours (c), and 4 hours (d).

S6. Design and Sequences

The detailed design of the rectangular origami core is presented in Figure S35. The four edges are kept unhybridized to facilitate future linking. The single-stranded loops on the left and right edges of the rectangular core also prevent the monomers from blunt end stacking[14]. Coordinates are added to identify the staples. The functionalization sites of FAM and TAMRA are also marked.

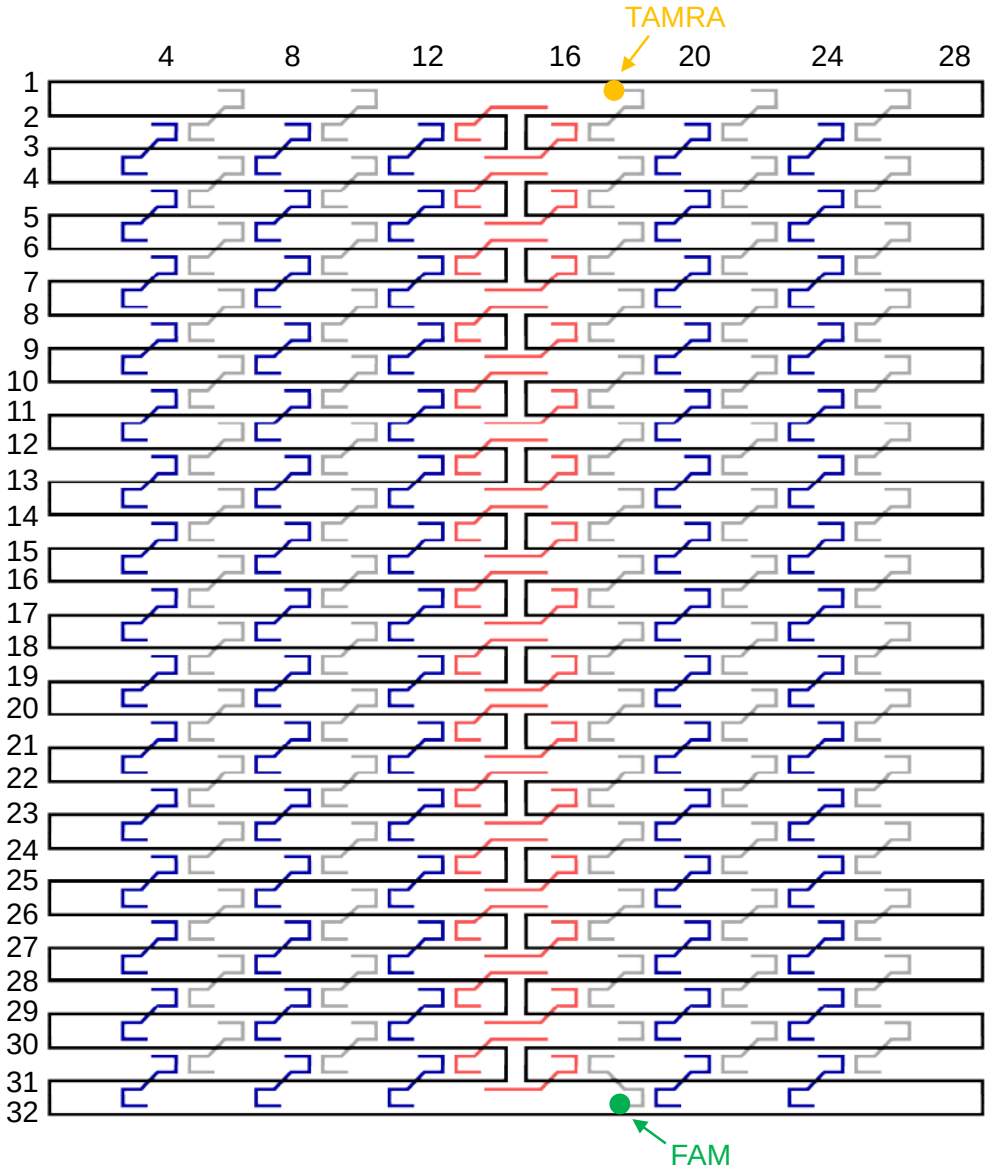

Figure S35: Folding path diagram of the original 32-helix rectangular origami.

Staple sequences for origami monomer core

Blue staples		Gray staples	
Name	Sequence	Name	Sequence
[02,04]	TGAGTTTCAAAGGAACAACTAAAGATCTCCAA	[01,06]	GAGAATAGGTCACCAGTACAAACTCCGCCACC
[02,08]	TGTAGCATAACTTTCAACAGTTTCTAATTGTA	[01,10]	TGCTAAACTCCACAGACAGCCCTCTACCGCCA
[02,12]	CGTAACGAAAATGAATTTTCTGTAGTGAATTT	[01,18]*	TAAGCGTCGGTAATAAGTTTTAACCCGTCGAG-TAMRA
[02,20]	TGCCTTGACAGTCTCTGAATTTACCCCTCAGA	[01,22]	GGAAAGCGGTAACAGTGCCCGTATCGGGGTTT
[02,24]	AATGCCCCATAAATCCTCATTAAAAGAACCAC	[01,26]	ACAAACAACTGCCTATTTCGGAACCTGAGACT
[04,04]	AAATTTTAAAGGCTTTTGCGGGATCGTCGGGTAGCA	[03,06]	AAAGGCCGCTCCAAAAGGAGCCTTAGCGGAGT
[04,08]	TCGGTTTAGGTCGCTGAGGCTTGCAAAGACTT	[03,10]	ATATATTCTCAGCTTGCTTTCGAGTGGGATTT
[04,12]	CTTAAACAACAACCATCGCCCACGCGGGTAAA	[03,18]	AACCAGAGACCCTCAGAACCGCCACGTTCCAG
[04,20]	GCCACCACTCTTTTCATAATCAAATAGCAAGG	[03,22]	GTTTGCCACCTCAGAGCCGCCACCGCCAGAAT
[04,24]	CACCAGAGTTCGGTCATAGCCCCCTCGATAGC	[03,26]	TCGGCATTCCGCCGCCAGCATTGATGATATTC
[06,04]	ACGGCTACAAGTACAACGGAGATTCGCGACCT	[05,06]	GCGAAACAAGAGGCTTTGAGGACTAGGGAGTT
[06,08]	TTTCATGATGACCCCCAGCGATTAAGGCGCAG	[05,10]	CTCATCTTGGAAGTTTCCATTAAACATAACCG
[06,12]	ATACGTAAGAGGCAAAAGAATACACTGACCAA	[05,18]	GACTTGAGGTAGCACCATTACCATATCACCGG
[06,20]	CCGGAAACTAAAGGTGAATTATCATAAAAGAA	[05,22]	TTATTCATGTCACCAATGAAACCATTATTAGC
[06,24]	AGCACCGTAGGGAAGGTAAATATTTTATTTTG	[05,26]	ATTGAGGGAATCAGTAGCGACAGACGTTTTCA
[08,04]	GCTCCATGACGTAACAAAGCTGCTACACCAGA	[07,06]	CCAAATCATTACTTAGCCGGAACGTACCAAGC
[08,08]	ACGGTCAATGACAAGAACCGGATATGGTTTAA	[07,10]	AGTAATCTTCATAAGGGAACCGAACTAAAACA
[08,12]	CTTTGAAAATAGGCTGGCTGACCTACCTTATG	[07,18]	TTATTACGTAAAGGTGGCAACATACCGTCACC
[08,20]	ACGCAAAGAAGAACTGGCATGATTTGAGTTAA	[07,22]	ATACCCAAACACCACGGAATAAGTGACGGAAA
[08,24]	TCACAATCCCGAGGAAACGCAATAATGAAATA	[07,26]	GAAGGAAAAATAGAAAATTCATATTTCAACCG
[10,04]	ACGAGTAGATCAGTTGAGATTTAGCGCCAAAA	[09,06]	AAAGATTCTAAATTGGGCTTGAGATTCATTAC
[10,08]	TTTCAACTACGGAACAACATTATTAACACTAT	[09,10]	ACGAACTATTAATCATTGTGAATTTCATCAAG
[10,12]	CGATTTTAGGAAGAAAAATCTACGGATAAAAA	[09,18]	TGAACAAAGATAACCCACAAGAATAAGACTCC
[10,20]	GCCCAATAGACGGGAGAATTAACTTTCCAGAG	[09,22]	GCGCATTAATAAGAGCAAGAAACAATAACGGA
[10,24]	GCAATAGCAGAGAATAACATAAAAACAGCCAT	[09,26]	CTTTACAGTATCTTACCGAAGCCCAGTTACCA
[12,04]	GGAATTACCATTGAATCCCCCTCACCATAAAT	[11,06]	TAAATATTGAGGCATAGTAAGAGCACAGGTAG
[12,08]	CATAACCCGCGTCCAATACTGCGGTATTATAG	[11,10]	ACTGGATATCGTTTACCAGACGACTTAATAAA
[12,12]	CCAAAATAAGGGGGTAATAGTAAATTTTAAAAGATT	[11,18]	TATTTTGCACGCTAACGAGCGTCTGAACACCC
[12,20]	CCTAATTTAAGCCTTAAATCAAGAATCGAGAA	[11,22]	AGGTTTTGGCCAGTTACAAAATAAACAGGGAA
[12,24]	ATTATTTATTAGCGAACCTCCCGACGTAGGAA	[11,26]	GAGGCGTTTCCCAATCCAAATAAGATAGCAGC
[14,04]	CAAAAATCATTGCTCCTTTTGATAATTGCTGA	[13,06]	TACCTTTAAGGTCTTTACCCTGACAATCGTCA
[14,08]	TCAGAAGCCTCCAACAGGTCAGGATTTAAATA	[13,10]	GAAGCAAATTTTAAAGCGGATTGCATCAATGTTTAG
[14,12]	AAGAGGAACGAGCTTCAAAGCGAAAGTTTCAT	[13,18]	ATCGGCTGACCAAGTACCGCACTCTTAGTTGC
[14,20]	CAAGCAAGCGAGCATGTAGAAACCAGAGAATA	[13,22]	CTAATTTACCGTTTTTATTTTCATCTTGCGGG
[14,24]	TCATTACCGAACAAGAAAAATAATAATTCTGT	[13,26]	TAAGTCCTGCGCCCAATAGCAAGCAAGAACGC
[16,04]	ATATAATGGGGGCGCGAGCTGAAATTAACATC	[15,06]	TTTCATTTCTGTAGCTCAACATGTTTAGAGAG

[16,08]	TGCAACTAGGTCAATAACCTGTTTAGAATTAG	[15,10]	TCGCAAATAAGTACGGTGTCTGGACCAGACCG
[16,12]	TCCATATATTTAGTTTGACCATTAAGCATAAA	[15,18]	CATATTTATTTCGAGCCAGTAATAAATCAATA
[16,20]	TAAAGTACCAGTAGGGCTTAATTGCTAAATTT	[15,22]	ACGCTCAACGACAAAAGGTAAAGTATCCCATC
[16,24]	CCAGACGACAAATTCTTACCAGTAGATAAATA	[15,26]	GCGTTATACGACAATAAACAACATACAATAGA
[18,04]	CAATAAATAAATGCAATGCCTGAGAAGGCCGG	[17,06]	TATATTTTCATACAGGCAAGGCAAAGCTATAT
[18,08]	CAAAATTAGGATAAAAATTTTTAGGATATTCA	[17,10]	CAACGCAAAGCAATAAAGCCTCAGGATACATT
[18,12]	GCTAAATCCTTTTGCGGGAGAAGCCCGGAGAG	[17,18]	ACAAAGAAAATTTCATCTTCTGACAGAATCGC
[18,20]	AATGGTTTTGCTGATGCAAATCCATTTTCCCT	[17,22]	TATGTAAAGAAATACCGACCGTGTTAAAGCCA
[18,24]	AGGCGTTAGGCTTAGGTTGGGTTAAGCTTAGA	[17,26]	TAACCTCCAATAAGAATAAACACCTATCATAT
[20,04]	AGACAGTCTCATATGTACCCCGGTTTGTATAA	[19,06]	CATGTCAAAAATCACCATCAATATAACCCTCA
[20,08]	ACCGTTCTGATGAACGGTAATCGTAATATTTT	[19,10]	AGAGAATCAGCTGATAAATTAATGCTTTATTT
[20,12]	GGTAGCTATTGCCTGAGAGTCTGGTTAAATCA	[19,18]	AAATCAATCGTCGCTATTAATTAAATCGCAAG
[20,20]	TAGAATCCCCTTTTTTAATGGAAACGGATTCG	[19,22]	TTGAATTATTGAAAACATAGCGATTATAACTA
[20,24]	TTAAGACGATTAATTACATTTAACACAAAATC	[19,26]	AAAACAAACTGAGAAGAGTCAATATACCTTTT
[22,04]	GCAAATATGATTCTCCGTGGGAACCGTTGGTG	[21,06]	ACCCGTCGTTAAATTGTAAACGTTAAAACTAG
[22,08]	GTTAAAATAACATTAAATGTGAGCATCTGCCA	[21,10]	CTTTCATCTCGCATTAAATTTTTGAGCAAACA
[22,12]	GCTCATTTCGCGTCTGGCCTTCCTGGCCTCAG	[21,18]	TTTAACGTTCGGGAGAAACAATAACAGTACAT
[22,20]	CCTGATTGAAAGAAATTGCGTAGAAGAAGGAG	[21,22]	ACAGAAATCTTTGAATACCAAGTTAATTTCAT
[22,24]	GCGCAGAGATATCAAAATTATTTGTATCAGAT	[21,26]	AACCTACCGCGAATTATTCATTTCACATCAAG
[24,04]	TAGATGGGGTGCGGGCCTCTTCGCGCAAGGCG	[23,06]	GGCGATCGCGCATCGTAACCGTGCGAGTAACA
[24,08]	GTTTGAGGTCAGGCTGCGCAACTGTTCCCAGT	[23,10]	TTCGCCATGGACGACGACAGTATCGTAGCCAG
[24,12]	GAAGATCGTGCCGGAAACCAGGCAGTGCCAAG	[23,18]	TTATTAATGAACAAAGAAACCACCTTTTCAGG
[24,20]	CGGAATTACGTATTAAATCCTTTGGTTGGCAA	[23,22]	CGACAACTTCATCATATTCCTGATCACGTAAA
[24,24]	GATGGCAAAAGTATTAGACTTTACAAGGTTAT	[23,26]	GGATTTAGTTCATCAATATAATCCAGGGTTAG
[26,04]	ATTAAGTTTTCCACACAACATACGCCTAATGA	[25,06]	GCTCACAAGGGTAACGCCAGGGTTTTGGGAAG
[26,08]	CACGACGTGTTTCCTGTGTGAAATTTGCGCTC	[25,10]	TCATAGCTTGTAAAACGACGGCCAAAGCGCCA
[26,12]	CTTGCATGCCGAGCTCGAATTCGTCCTGTCGT	[25,18]	CTAAAGCAAATCAATATCTGGTCACCCGAACG
[26,20]	ATCAACAGGAGAGCCAGCAGCAAAATATTTTT	[25,22]	GCCACGCTTTGAAAGGAATTGAGGAAACAATT
[26,24]	CTAAAATAAGTATTAACACCGCCTCGAACTGA	[25,26]	AGGCGGTCTCTTTAGGAGCACTAAACATTTGA
[28,04]	GTGAGCTAGCCCTTCACCGCCTGGGGTTTGCC	[27,06]	AGCTGATTACTCACATTAATTGCGTGTTATCC
[28,08]	ACTGCCCGCTTTTCACCAGTGAGATGGTGGTT	[27,10]	TGGTTTTTCTTTCCAGTCGGGAAAAATCATGG
[28,12]	GCCAGCTGCGGTTTGCGTATTGGGAATCAAAA	[27,18]	GCCAACAGATACGTGGCACAGACATGAAAAAT
[28,20]	GAATGGCTACCAGTAATAAAAGGGCAAACTAT	[27,22]	GTCACACGATTAGTCTTTAATGCGGCAACAGT
[28,24]	TAGCCCTATTATTTACATTGGCAGCAATATTA	[27,26]	GAAATGGAAAACATCGCCATTAAACAGAGGTG
[30,04]	CCAGCAGGCGATGGCCCACTACGTGAGGTGCC	[29,06]	TATCAGGGCGAAAATCCTGTTTGACGGGCAAC
[30,08]	CCGAAATCAACGTCAAAGGGCGAAAAGGGAGC	[29,10]	TGGACTCCGGCAAAATCCCTTATACGCCAGGG
[30,12]	GAATAGCCACAAGAGTCCACTATTAAGCCGGC	[29,18]	GAAGAACTACATTCTG
[30,20]	CGGCCTTGGTCTGTCCATCACGCATTGACGAG	[29,22]	GTAAAAGACTGGTAATATCCAGAAATTCACCA
[30,24]	CCGCCAGCTTTTATAATCAGTGAGAGAATCAG	[29,26]	AGAAGTGTCATTGCAACAGGAAAATTTTAATCGTCT

Red staples		Special staples	
Name	Sequence	[32,18]*	FAM-AAGAACTACATTCTGTACAGGGCGCGTACTA
seam[02,13]	ACGTTAGTTCTAAAGTTTTGTCGTGATACAGG		
seam[02,16]	AGTGTACTATACATGGCTTTTGATCTTTCCAG		
seam[04,13]	CAATGACAGCTTGATACCGATAGTCTCCCTCA		
seam[04,16]	GAGCCGCCCCACCACCGGAACCGCTGCGCCGA		
seam[06,13]	AAACGAAATGCCACTACGAAGGCAGCCAGCAA		
seam[06,16]	AATCACCACCATTTGGGAATTAGACCAACCTA		
seam[08,13]	CCAGGCGCGAGGACAGATGAACGGGTAGAAAA		
seam[08,16]	TACATACACAGTATGTTAGCAAACTGTACAGA		
seam[10,13]	GGACGTTGAGAACTGGCTCATTATGCGCTAAT		
seam[10,16]	ATCAGAGAGTCAGAGGGTAATTGAACCAGTCA		
seam[12,13]	TTTGCCAGGCGAGAGGCTTTTGCAATCCTGAA		
seam[12,16]	TCTTACCAACCCAGCTACAATTTTAAAGAAGT		
seam[14,13]	TTTTAATTGCCCGAAAGACTTCAACAAGAACG		
seam[14,16]	GGTATTAATCTTTCCTTATCATTCATATCGCG		
seam[16,13]	CGAGTAGAACAGTTGATTCCCAATATTTAGGC		
seam[16,16]	AGAGGCATACAACGCCAACATGTATCTGCGAA		
seam[18,13]	CTGTAATAGGTTGTACCAAAAACACAAATATA		
seam[18,16]	TTTTAGTTCGCGAGAAAACTTTTTTTATGACC		
seam[20,13]	TCAGGTCATTTTTGAGAGATCTACCCTTGCTT		
seam[20,16]	CTGTAAATATATGTGAGTGAATAAAAAGGCTA		
seam[22,13]	AAATAATTTTTAACCAATAGGAACAACAGTAC		
seam[22,16]	CTTTTACACAGATGAATATACAGTGCCATCAA		
seam[24,13]	GCTTCTGGCACTCCAGCCAGCTTTACATTATC		
seam[24,16]	ATTTTGCGTTTAAAAGTTTGAGTACCGGCACC		
seam[26,13]	CCCGGGTACCTGCAGGTCGACTCTCAAATATC		
seam[26,16]	AAACCCTCTCACCTTGCTGAACCTAGAGGATC		
seam[28,13]	GGGAGAGGCATTAATGAATCGGCCACCTGAAA		
seam[28,16]	GCGTAAGAAGATAGAACCCTTCTGAACGCGCG		
seam[30,13]	AGTTTGGACGAGATAGGGTTGAGTGTAATAAC		
seam[30,16]	ATCACTTGAATACTTCTTTGATTAGTTGTTCC		

Sequences of toehold-decorated vertical linkers

Name	Sequence
vlinker1	CCATACGTCAAGCCCACAAGTTTTTTGGGGTCGAACCATCCCATCCAG
vlinker2	GTGTTTACCTCAGAGCCTAAATCGGAACCCTAAAACCGTCGTGTTGGG
vlinker3	TCAGAGCGCCCTCAGATAGAGCTTGACGGGGAAAAGAACGCCATCTTT
vlinker4	CGGCATCAAGGGTTGAGCGTACTATGGTTGCTAATTAACCGCGAATCC
vlinker5	CGGGATCGTGCTCAGTACGTGCTTTCCTCGTTGCCACCGATGGATAGC
vlinker6	GTATTCGGCCTCAAGACTAAACAGGAGGCCGAGAATCCTGTAACAGCC
vlinker7	GTTCAGATGTAAAGCACACCACCCTCATTTTCCGTAACACGTCTAAGA
vlinker8	CCGACTTGCCCCGATTACCGCCACCCTCAGAAACAACGCCTAGGAACC
vlinker9	TCAACACAGAACGTGGTACTCAGGAGGTTTAGATAGTTAGCTTCTGGA
vlinker10	ATTCCCTCCACGTATAACCAGGCGGATAAGTGGGGGTCAGAGTAGGAT
vlinker11	ACAACAGTAGCGGGAGGAAGGATTAGGATTAGAAACAGTTCTTAAAGC
vlinker12	CTGCGAAGATTTTAGATGAAAGTATTAAGAGGCTATTATTGCGGGTTG
vlinker13	CGGTTTCCTATCACCGCGAGAAAGGAAGGGAATGCGCCGCTCAACCAA

Sequences of releasers

Name	Sequence
releaser1	CTGGATGGGATGGTTCGACCCCAAAAAACTTGTGGGCTTGACGTATGG
releaser2	CCCAACACGACGGTTTTAGGGTTCCGATTTAGGCTCTGAGGTAAACAC
releaser3	AAAGATGGCGTTCTTTTCCCCGTCAAGCTCTATCTGAGGGCGCTCTGA
releaser4	GGATTCGCGGTTAATTAGCAACCATAGTACGCTCAACCCTTGATGCCG
releaser5	GCTATCCATCGGTGGCAACGAGGAAAGCACGTACTGAGCACGATCCCG
releaser6	GGCTGTTACAGGATTCTCGGCCTCCTGTTTAGTCTTGAGGCCGAATAC
releaser7	TCTTAGACGTGTTACGGAAAATGAGGGTGGTGTGCTTTACATCTGAAC
releaser8	GGTTCCTAGGCGTTGTTTCTGAGGGTGGCGGTAATCGGGGCAAGTCGG
releaser9	TCCAGAAGCTAACTATCTAAACCTCCTGAGTACCACGTTCTGTGTTGA
releaser10	ATCCTACTCTGACCCCCACTTATCCGCCTGGTTATACGTGGAGGGAAT
releaser11	GCTTTAAGAACTGTTTCTAATCCTAATCCTTCCTCCCGCTACTGTTGT
releaser12	CAACCCGCAATAATAGCCTCTTAATACTTTCATCTAAAATCTTCGCAG
releaser13	TTGGTTGAGCGGCGCATTCCCTTCCTTTCTCGCGGTGATAGGAAACCG

Sequences of horizontal linkers

Name	Sequence
hlinker1	CAGCGAAAGCGTCAGACTGTAGCGATCAAGTT
hlinker2	GAATAAGGGCAGATAGCCGAACAATTTTTAAG
hlinker3	AAACAGTTGCTTATCCGGTATTCTAAATCAGA
hlinker4	TCAATTCTGAAAAAGCCTGTTTAGGGAATCAT
hlinker5	AGAAAAGCGAAGATGATGAAACAAAATTACCT
hlinker6	CAGCTGGCGCCGTCAATAGATAATCAACTAAT
hlinker7	GAGTTGCACTACATTTTGACGCTCACGCTCAT
hlinker8	TGCCTTTAGACAGCATCGGAACGAACCCTCAG
hlinker9	AAAAGTAACTTGCCCTGACGAGAACATTCAGT
hlinker10	TATAGAAGCAGAAAACGAGAATGAAATGCTTT
hlinker11	AATTACTAACTAATAGTAGTAGCAAGGTGGCA
hlinker12	GAGCAAAACCCAAAAACAGGAAGATGATAATC
hlinker13	AGATTAGAGAAAGGGGGATGTGCTTATTACGC

S7. References

(1) Jacobson, H.; Stockmayer, W. H. *J. Chem. Phys.* **1950**, *18*, 1600.

(2) Podtelezhnikov, A. A.; Mao, C. D.; Seeman, N. C.; Vologodskii, A. *Biophysical Journal* **2000**, *79*, 2692.

(3) Sa-Ardyen, P.; Vologodskii, A. V.; Seeman, N. C. *Biophysical Journal* **2003**, *84*, 3829.

(4) Koo, H. S.; Drak, J.; Rice, J. A.; Crothers, D. M. *Biochemistry* **1990**, *29*, 4227.

(5) Shore, D.; Langowski, J.; Baldwin, R. L. *Proceedings of the National Academy of Sciences of the United States of America-Biological Sciences* **1981**, *78*, 4833.

(6) Kim, D. N.; Kilchherr, F.; Dietz, H.; Bathe, M. *Nucleic Acids Research* **2012**, *40*, 2862.

(7) Castro, C. E.; Kilchherr, F.; Kim, D. N.; Shiao, E. L.; Wauer, T.; Wortmann, P.; Bathe, M.; Dietz, H. *Nat. Methods* **2011**, *8*, 221.

(8) Timoshenko, S.; Goodier, J. *Theory of elasticity, 1987*; McGraw-Hill, New York.

(9) Laurendeau, N. M. *Statistical thermodynamics: fundamentals and applications*; Cambridge University Press, 2005.

(10) Moffat, R. J. *Experimental thermal and fluid science* **1988**, *1*, 3.

(11) Soong, T. T. *Fundamentals of probability and statistics for engineers*; John Wiley & Sons, 2004.

(12) Lakowicz, J. R. *Principles of fluorescence spectroscopy*; Springer, 2007.

(13) SantaLucia, J. *Proceedings of the National Academy of Sciences of the United States of America* **1998**, *95*, 1460.

(14) Rothemund, P. W. K. *Nature* **2006**, *440*, 297.